

Achterberg Eric, Pieter (Orcid ID: 0000-0002-3061-2767)
Klar Jessica, K (Orcid ID: 0000-0003-1025-4859)
Browning Thomas, J. (Orcid ID: 0000-0002-2864-6087)
Marsay Christopher, M. (Orcid ID: 0000-0003-1244-0444)
Painter Stuart, C. (Orcid ID: 0000-0001-7934-7346)
Baker Alex, R. (Orcid ID: 0000-0002-8365-8953)
Hamilton Douglas, Stephen (Orcid ID: 0000-0002-8171-5723)
Tanhua Toste (Orcid ID: 0000-0002-0313-2557)

Trace element biogeochemistry in the high latitude North Atlantic Ocean: seasonal variations and volcanic inputs

Eric P. Achterberg^{1,2}, Sebastian Steigenberger^{1,3}, Jessica K. Klar⁴, Thomas J. Browning², Chris M. Marsay⁵, Stuart C. Painter³, Lúcia H. Vieira², Alex R. Baker⁶, Douglas S. Hamilton⁷, Toste Tanhua², C. Mark Moore¹

¹Earth and Ocean Science, National Oceanography Centre Southampton, University of Southampton, Southampton SO14 3ZH, UK

²GEOMAR Helmholtz Centre for Ocean Research Kiel, 24148, Germany

³National Oceanography Centre, Southampton SO14 3ZH, UK

⁴Centre de Formation et de Recherche sur les Environnements Méditerranéens (CEFREM), UMR 5110, Université de Perpignan Via Domitia, CNRS, 66860 Perpignan Cedex, France

⁵Skidaway Institute of Oceanography, University of Georgia, Savannah, GA 31411, USA

⁶School of Environmental Sciences, University of East Anglia, Norwich, UK

⁷Department of Earth and Atmospheric Science, Cornell University, Ithaca, NY, USA

Corresponding author: Eric P. Achterberg (eachterberg@geomar.de)

Key Points:

- Bio-essential element concentrations in surface waters decreased from spring to summer with removal ratios reflecting biological uptake
- Effects of volcanic inputs from Eyjafjallajökull in spring 2010 were pronounced for Al, Mn and Zn but returned to typical levels in summer
- Deep winter convection dominated trace element supply to surface waters with minor contributions from atmospheric and diffusive mixing

Abstract

We present dissolved and total dissolvable trace elements for spring and summer cruises in 2010 in the high latitude North Atlantic. Surface and full depth data are provided for Al, Cd, Co, Cu, Mn, Ni, Pb, Zn in the Iceland and Irminger Basins, and consequences of biological uptake and inputs by the spring Eyjafjallajökull volcanic eruption are assessed. Ash from Eyjafjallajökull resulted in pronounced increases in Al, Mn and Zn in surface waters in close proximity to Iceland during the eruption, whilst 3 months later during the summer cruise levels had returned to more typical values for the region. The apparent seasonal removal ratios of surface trace elements were

This article has been accepted for publication and undergone full peer review but has not been through the copyediting, typesetting, pagination and proofreading process which may lead to differences between this version and the Version of Record. Please cite this article as doi: 10.1029/2020GB006674

consistent with biological export. Assessment of supply of trace elements to the surface mixed layer for the region, excluding volcanic inputs, indicated that deep winter mixing was the dominant source, with diffusive mixing being a minor source (between 13.5% (dissolved Cd (DCd)) and -2.43% (DZn) of deep winter flux), and atmospheric inputs being an important source only for DAl and DZn (DAl up to 42% and DZn up to 4.2% of deep winter+diffusive fluxes) and typically less than 1% for the other elements. Elemental supply ratios to the surface mixed layer through convection were comparable to apparent removal ratios we calculated between spring and summer. Given that deep mixing dominated nutrient and trace element supply to surface waters, predicted increases in water column stratification in this region may reduce supply, with potential consequences for primary production and the biological carbon pump.

1 Introduction

Primary productivity, standing stock, species composition and trophic structure of planktonic communities in the oceans are controlled by the availability of light, macronutrients (nitrogen (N), phosphorus (P) and silicon (Si)) and the micronutrient iron (Fe), in association with loss processes by viral lysis and zooplankton grazing (Boyd et al., 2007; Graziano et al., 1996; Martin, 1991; Nelson et al., 2001; Wu et al., 2000). These controls influence export production and thereby impact the global carbon cycle (Brix et al., 2006). Trace elements other than Fe also play an important role in the functioning of microbial organisms, with the next most abundant trace elements in marine phytoplankton after Fe being (in order) zinc (Zn), manganese (Mn), copper (Cu), nickel (Ni), cadmium (Cd) and cobalt (Co) (Twining and Baines, 2013).

These micronutrient trace metals play key roles in a range of cellular processes that ultimately determine rates of oceanic primary productivity (Morel and Price, 2003). The availability of these micronutrient elements can therefore influence the fixation of CO₂, generation of O₂, uptake of N, P and Fe, with enhanced levels potentially resulting in toxic effects (Morel and Price, 2003). The involvement in biological processes results in a removal of micronutrients like Cd, Cu, Ni and Zn from the surface ocean by microbial organisms, with release at depth following remineralisation of sinking particles (Bruland and Lohan, 2004).

The supply and removal processes of the oceanic micronutrients can be elucidated with the use of tracers, such as aluminium (Al) for dust inputs (Vink and Measures, 2000), Mn for benthic supply (Laës et al., 2007), and lead (Pb) for scavenging (Kadko, 1993). We still have a limited understanding of the oceanic distributions and cycling of trace elements, despite their important biogeochemical roles. In recent years, large new datasets have emerged as part of the international GEOTRACES programme (Henderson et al., 2007; Schlitzer et al., 2018). The availability of oceanic Fe data has substantially improved (e.g.(Fitzsimmons and others, 2017; Milne et al., 2017; Tagliabue et al., 2012)), with also some new datasets for e.g. Zn (Middag et al., 2019; Wyatt et al., 2014), Al (Measures et al., 2015; Menzel Barraqueta et al., 2018), Pb (Noble et al., 2015; Rusiecka et al., 2018), Cd (Middag et al., 2018; Wu and Roshan, 2015) and Ni (Middag et al., 2020).

The high latitude North Atlantic Ocean features a pronounced annual spring bloom (Sanders et al., 2005) and has areas of deep water formation, and therefore forms an

important component of the oceanic carbon cycle (Broecker, 1991; Pickart et al., 2003). The typical annual phytoplankton bloom in the high latitude North Atlantic starts in early April and lasts towards mid-May, with a second peak towards the end of June, followed by chlorophyll a levels decreasing afterwards (Sanders et al., 2005; Achterberg et al., 2013). The region has become a focus for research into the role of Fe in ocean productivity, community structure and carbon export (Browning et al., 2019; Giering et al., 2012; Le Moigne et al., 2014; Moore et al., 2006; Nielsdottir et al., 2009; Ryan-Keogh et al., 2013). Residual nitrate concentrations have been observed during late spring and summer in surface waters of the high latitude North Atlantic (Moore et al., 2006; Nielsdottir et al., 2009), indicating a reduced efficiency of the biological carbon pump (Sarmiento and Toggweiler, 1984). Limitation of phytoplankton growth, resulting in the residual nitrate levels, has been attributed to a limited supply and availability of Fe (Achterberg et al., 2013, 2018; Nielsdottir et al., 2009; Ryan-Keogh et al., 2013).

This study is part of the Irminger Basin Iron Study (IBIS) and presents the distributions of dissolved and total dissolvable Al, Cd, Cu, Mn, Ni, Pb and Zn, and the quantification of their various sources to and removal mechanisms from the surface ocean of the high latitude North Atlantic. The geographical focus of IBIS was the Iceland Basin (IB) and Irminger Basin (IRB). Research cruises in different seasons (spring and summer) as part of IBIS were conducted during and after an eruption of the Eyjafjallajökull volcano which impacted the study region (Achterberg et al., 2013). The study therefore allowed for a unique seasonal perspective of the effects of trace element cycling in the study region, including a direct assessment of volcanic inputs, for which some indirect but few direct observations exist, e.g. (Duggen et al., 2007; Hamme et al., 2010; Lin et al., 2011). A recent paper has reported on the distributions of dissolved and dissolvable Fe in the study region as part of IBIS Programme (Achterberg et al., 2018). Here we present multiple elements other than Fe, providing a thorough comparison of their biogeochemical cycles in this study region.

2 Materials and Methods

2.1 Sample collection

Water samples were obtained in the high latitude North Atlantic at 41 full depth CTD casts and 195 underway surface stations during cruises D350, D351 and D354 on board RRS *Discovery*. The cruises took place in spring and summer 2010 (Spring: April 26-May 9 (D350) and May 10-28 (D351); Summer: July 4-August 11 (D354)) (cruise tracks in Supporting Information (SI) Fig. S1). The samples were collected in the shelf regions off Iceland (D350, D351, D354) and Greenland (D354), and in the IB (D350, D351, D354) and IRB (D350, D354) (Fig. 1). The spring cruises D350 and D351 were conducted during the explosive eruption phase of the Eyjafjallajökull volcano, and the summer cruise sailed following the eruption (Achterberg et al., 2013). All data are available from the British Oceanographic Data Centre.

Samples were collected using trace metal clean 10 L OTE (Ocean Test Equipment) Niskin samplers mounted on a Ti CTD rosette frame. The OTE bottles were immediately transferred into a pressurized clean container (class 1000) for sub-sampling. In addition, surface seawater (~3 m depth) was pumped from a tow fish into the clean container using a Teflon diaphragm pump (Almatec A15) connected to a

clean oil-free air compressor (JunAir) (Achterberg et al., 2001) and samples taken every two hours whilst the ship was in transit.

Samples for trace metal analysis were collected in acid-cleaned 125 or 250 ml low-density polyethylene bottles (LDPE, Nalgene) after on-line filtration with a 0.2 μm cartridge filter (with 0.45 μm pre-filter, Sartobran 300, Sartorius). The samples from the OTE bottles were filtered under pure N_2 pressure (filtered 99.99% N_2 , 1 bar), whereas those from the tow fish were filtered using the pressure from the Teflon pump. Additional samples were collected without filtration. Each sample was acidified to pH \sim 1.9 on board in a laminar flow hood (class 100) with nitric acid (UpA HNO_3 , Romil, UK) and stored in double bags until analysis at the National Oceanography Centre Southampton. The storage of the acidified (pH \sim 1.9) unfiltered samples with subsequent analysis after 18 months yielded total dissolvable metal (TDAI, TDCd, TDCo, TDCu, TDMn, TDNi, TDPb, TDZn) concentrations, which include the dissolved (0.2 μm filtered) and an acid leachable fraction of the particulate pool (no TDAI data available for tow fish surface samples). In order to verify that sampling and sample handling procedures were trace metal clean, samples were analysed for dissolved Fe (DFe) at sea using a flow injection technique (Obata et al., 1993).

2.2 Trace metal and nutrient analysis

Concentrations of trace metals were determined by isotope dilution inductively coupled mass spectrometry (ID-ICP-MS), whilst the mono-isotopic elements Co and Mn were analysed using a standard addition approach followed by ICP-MS detection; all according to methods described in (Rapp et al., 2017). Full details are supplied in the in SI (Text S1). The values determined using the ICP-MS method showed good consistency with the reported consensus values for the elements (SI, Table S1). Aluminium in seawater was determined using a flow injection lumogallion method with fluorescence detection (Brown and Bruland, 2008); full details in SI (Text S1). Nitrate+nitrite (Total Oxidised Nitrogen: TON), silicic acid and phosphate were analysed at sea using standard auto-analyser techniques (Grasshoff et al., 1983) on a Skalar instrument, following the best practice guide for performing nutrient measurements at sea (Hydes et al., 2010).

2.3 Aerosol sampling and analysis

During the spring, aerosol samples were collected onto single 20 x 25 cm Whatman 41 filters (Fisher) using a high volume aerosol collector (Tisch TSP) operating at a flow rate of ca. $1 \text{ m}^3 \text{ min}^{-1}$ (Baker et al., 2007) and located on the deck above the bridge of RRS *Discovery*. Separation of particles into aerodynamic diameters greater than or less than 1 μm was achieved during the summer cruise using a Sierra-type cascade impactor, also using Whatman 41 (Fisher) slotted substrates and filters. Collection filters and slotted substrates were acid-washed before use with 0.5 M HCl (Aristar Grade, Fisher), followed by 0.1 M HCl (Aristar Grade, Fisher). Collection times for most samples were relatively long (2-3 days) because of low aerosol trace metal concentrations in the high latitude North Atlantic, but samples collected under the Eyjafjallajokull ash plume (spring TM07-09; locations of aerosol sampling depicted in Fig. S2 (SI)) were only collected for 1–3 hours. The collector was only used when the ship was heading into the prevailing wind in order to avoid contamination from the vessel.

Following collection, samples were sealed in plastic bags and immediately frozen at -20°C for return to the land-based laboratory. Trace elements were leached from the

filters using a 1 M ammonium acetate solution (pH 4.7) and filtered through 0.2 μm filters (Minisart, Sartorius) (Baker et al., 2007) and their soluble concentrations were determined by ICP-OES and ICP-MS (Baker and Jickells, 2017). Total element concentrations were determined on portions of the filters by instrumental neutron activation analysis (INAA), with the two size fractions for the summer cruise samples combined together to give a single measurement (Sholkovitz et al., 2012) (Pb cannot be determined by INAA). Here we report on the dry deposition fluxes of soluble elements (F_{dry} , $\text{nmol m}^{-2} \text{d}^{-1}$) as the product of their aerosol concentrations (C_{aero} , pmol m^{-3}) and a dry deposition velocity (v_d) ($F_{\text{dry}} = C_{\text{aero}} v_d$). Values of v_d were set to 1 and 0.1 cm s^{-1} for the coarse ($> 1 \mu\text{m}$) and fine ($< 1 \mu\text{m}$) aerosol modes, respectively for summer cruise, and 0.7 cm s^{-1} for the spring cruise (Baker et al., 2007; Ganzeveld et al., 1998). Deposition velocities vary strongly as a function of particle size and wind speed (Ganzeveld et al., 1998) and are highly uncertain. An uncertainty in v_d of plus or minus a factor of 2 – 3 has been reported (Duce et al., 1991).

Diffusive flux measurements and calculations

Turbulent kinetic energy dissipation (ϵ) was measured during summer cruise only using a free-fall microstructure shear profiler (MSS90L, Sea and Sun Technology GmbH). The rate of ϵ was calculated from the variance of the measured vertical microstructure shear by integration of the vertical microstructure shear power spectrum (Forryan et al., 2012) and assuming isotropic turbulence (Yamazaki and Osborn, 1990). Turbulent diffusivity (K) was estimated from ϵ and buoyancy frequency, full details of the approach are provided in (Painter et al., 2014). The top 8 m of data in the water column were omitted in order to remove near-surface influences prior to binning the diffusivity data into 4 m depth bins. Vertical diffusive fluxes of trace elements into surface mixed layer were subsequently determined from the turbulent diffusivity and profiles of the trace elements. The mixed layer depths (MLD) were obtained at the depth of the local maximum in the Brunt–Väisälä buoyancy frequency profile (MLD range 17–49 m, mean \pm 1 standard deviation: 28 ± 8 m) (Painter et al., 2014).

2.5 Winter Convective fluxes

Winter convective fluxes were obtained from examination of individual Argo float profiles from the IRB and IB in winter 2010, which allowed determination of the MLD using criteria by (de Boyer Montégut et al., 2004). The obtained mean winter MLD were 170 ± 100 m for the IRB and 355 ± 144 m for the IB, rounded to 200 and 350 m, respectively; full details are provided elsewhere (Painter et al., 2014). Dissolved metal concentrations from spring profiles in each basin were then integrated to the respective depth of winter mixing to obtain a mean estimate of convective inputs as reported previously (Nielsdottir et al., 2009). Limited spatial coverage of the IRB and IB by Argo floats introduced some uncertainty around the mean winter MLD which appeared spatially heterogenous whereas metal concentrations measured during the spring cruise at the mean winter MLD were more spatially homogenous. This latter observation suggests that convective fluxes obtained by blending mean winter MLD with spring metal concentrations is unlikely to be significantly in error due to the time gap between the two datasets.

3 Results and Discussion

3.1 Hydrography

The study region in the high latitude North Atlantic Ocean includes the IB and IRB, Hatton-Rockall Plateau, and Rockall Trough and Reykjanes Ridge regions (Fig. 1). The cyclonic subpolar gyre of the North Atlantic flows around the IRB and IB. The North Atlantic Drift (NAD) is part of the southern region of the subpolar gyre and flows as the main near-surface current northward into the central region of the high latitude North Atlantic (between ca. 10°W to 30°W) with depths in the IB of up to 1 km (Bower et al., 2002). The NAD is bounded by the cooler Irminger Current to the west, with the southern and eastern boundaries weakly constrained by extensions of the NAC (Rossby et al., 1998). The NAD has a salinity range of 35.2-35.7 and is warmer than surrounding waters (Rossby et al., 1998). The Irminger Current is prominent in the east IRB, and turns west in the north IRB before moving south in the subpolar gyre flow. Trajectories of Argo floats released in our study region during RRS *Discovery* cruise D321 (June 2007) indicate the described upper ocean current movements (in SI, Fig. S3). The western IRB features a fresh and cold western boundary current (East Greenland Current (EGC)) with a southerly flow, and salinity and temperature ranges of 30-34 and 3.5-5.5°C, respectively (Bacon et al., 2002).

Details of the water masses in our research area are discussed in the SI and shown in Table S2 (SI), and were used to support the interpretation of the potential temperature-salinity (θ -S) plot (SI, Fig. S4), optimum multiparameter (OMP) water mass analysis (Tomczak, 1999) for an east-west section along 60°N (SI, Fig. S5) and trace metal distributions.

3.2 Surface water distributions of dissolved and total dissolvable trace elements

A total of 195 surface samples were collected using the tow fish in the IB and IRB during the cruises. For off shore stations (water depth >400 m) the ranges and average surface water concentrations of nitrate+nitrite (TON), dissolved and total dissolvable trace elements for the spring and summer cruises are presented in Table 1, for the whole region and separately for the IB and IRB.

In surface waters, a gradient of decreasing TON and phosphate concentrations from northwest to southeast was observed for the spring cruises (Fig. 2). This trend was also observed for DAi, DCd, DCo, DCu, DN_i, DPb, DMn, DZn and was likely due to their active and/or passive biological uptake in relation to the general spatial progression of the spring bloom from east to west in the subpolar North Atlantic (Olsen et al., 2008), which was consistent with *in situ* and satellited derived chlorophyll data for 2013 (Ryan-Keogh et al., 2013). In addition, ash-derived metal inputs from the Eyjafjallajökull volcanic eruption phase during spring could have contributed to an increase in concentrations for a range of elements associated with the ash particles (Achterberg et al., 2013). There were elevated concentrations for a range of elements (DAi: 45 nM; DMn: 3.20 nM, TDMn 8.78 nM; DZn: 0.625 nM, TDZn 1.30 nM) directly under the volcanic plume (63.1°N, 18.5°W) in the immediate vicinity of the Icelandic coast (Table 1), but with no increases for Co, Cd, Cu, Ni and Pb compared with surface waters that were not influenced by the volcanic ash inputs (further discussion is

provided in aerosol section below). Enhanced DAl, DCd, DCo, DCu, DPb, DNi, DMn, DZn concentrations were also observed on the Scottish Shelf (Fig. 2), likely due to continental and benthic inputs; indeed the elevated DMn (8.73 nM) on this shelf provided a strong indication of benthic release (Birchill et al., 2019; Burdige, 1993).

Spatial variability in open ocean areas during spring was observed for surface water concentrations of trace metals (Fig. 2), which may be related to the temporal and spatial variability in ash deposition (Achterberg et al., 2013) and possibly (sub-) mesoscale processes, including fronts and eddies (Lévy et al., 2012). The total dissolvable metals showed similar patterns to dissolved metals, with generally lower concentrations in the southeast of the area where the bloom was already well progressed (Ryan-Keogh et al., 2013), but a less pronounced concentration increase towards the northwest (Fig. 2). The strongest relationships between dissolved and labile particulate elements (total dissolvable minus dissolved) were observed for Cd (-0.51), Cu (-0.57) and Ni (-0.54) (bivariate Pearson Correlation) indicating a transfer of the dissolved forms of these elements to particulate forms.

During the summer cruise (Fig. 3), phosphate and TON still showed a west to east decrease in concentrations, with anomalously high TON depletion in the IB, potentially as a result of the relief in Fe limitation of primary productivity by the additional Fe supply from volcanic ash inputs (Achterberg et al., 2013). Open ocean concentrations in the study region of DAl, DCd, DCo, DCu, DMn, DPb, DZn were lower than in spring (Figs. 2 and 3, Table 1). The coastal stations off Scotland and Iceland (Fig. 3) did not show elevated dissolved metal concentrations as observed during the spring cruises, with the reduction in concentrations likely the consequence of biological and physico-chemical removal (precipitation and scavenging for Al, Pb, Mn), and lower atmospheric inputs in the Icelandic waters following the termination of the Eyjafjallajökull eruption (May 22, 2010; (Gudmundsson et al., 2012)). Total dissolvable metal concentrations in the overall study region also showed reductions in average summer concentrations relative to spring (Fig. 2 and 3, Table 1), likely related to export of particles from the surface ocean. For the summer cruise strongest relationships between dissolved and labile particulate elements were observed for Cu (-0.70) with the rest of the elements showing $r < 0.29$.

Contributions of average dissolved to total dissolvable elemental concentration ratios for spring (first number) and summer (second number) were: Co (54%, 50%), Mn (50.5%, 60%), Ni (85%, 74%), Cd (69%, 21%), Pb (76%, 75%), Zn (43%, 16%), Cu (96%, 89%). This indicates that in the surface ocean Ni, Pb, Cu, (Cd spring only) were largely present in the dissolved forms, but around half or more of Co, Mn, Zn and Cd (Cd summer only) were in the particulate form, and likely incorporated in biogenic material (Cd, Zn; (Bruland et al., 2014)), or onto biogenic material through bacterial mediated precipitation (Mn, Co; (Moffett and Ho, 1996; Tebo et al., 2004)).

We compared average surface water dissolved and total dissolvable metal concentrations between the IB and IRB, as well as between spring and summer for the individual basins (Table 1). We included TON to determine the effects of biological uptake. The t-tests indicated significant differences in spring between the IB and IRB for DCd and DPb, and in summer for DCo, DCd, DCu and DNi, with lower concentrations in the IB compared with the IRB. Nitrate was also significantly lower in the IB compared to the IRB (by 1.34 fold in spring and 5 fold in summer), with the

depleted levels in the IB explained by enhanced TON removal as a result of the ash-derived Fe inputs (Achterberg et al., 2013) resulting in Fe and TON co-limited microbial communities (Ryan-Keogh et al., 2013).

For both the IRB and IB, all of the dissolved metals measured showed significant reductions in average summer concentrations relative to spring (Table 1). Furthermore, the t-tests indicated significant differences in spring between the IB and IRB for TDNi, and in summer for TDCd, TDNi and TDPb, with lower concentrations in the IB compared with the IRB (Table 1). Total dissolvable metal concentrations showed significant reductions for the individual basins in average summer concentrations relative to spring for Cd, Ni, Zn (IB only), Co, Cu, Pb (IB and IRB); but not for Mn (Table 1).

There is a paucity of surface ocean data for elements other than Fe and Al for our study region; comparison between our summer DAI data set (0.94 ± 0.837 nM (not influenced by volcanic ash inputs), Table 1) and that from a CLIVAR cruise (A16N in 2003, Al < 2 nM) indicates a reasonable agreement (Measures et al., 2008).

Mean values of the significant differences between spring and summer dissolved concentrations for multiple elements (Table 1), including Fe (Achterberg et al., 2018), could be used to calculate a net removal ratio (Table 2; in mmol metal:mol P). This apparent net export stoichiometry was very similar between the two basins for the majority of elements and, for the bio-essential metals (Fe, Ni, Zn, Cu, Fe, Cd, Mn, Co), was broadly consistent with what might be expected on the basis of biological dominance of removal (Twining and Baines, 2013). Interestingly, apparent Fe removal stoichiometry was higher in the IB than the IRB, potentially due to the more Fe limited status of the latter (Ryan-Keogh et al., 2013) and higher Fe inputs to the former (Achterberg et al., 2013).

3.3 Concentration profiles of dissolved and total dissolvable elements

Depth profiles of dissolved and total dissolvable elements for a station in the IRB are presented in order to illustrate the similarities and contrasts in their behaviours in the water column in the high latitude North Atlantic (Fig. 4).

The overall trend in dissolved Al, Cd, Co, Cu, Ni, and Zn shows depleted surface ocean concentrations with an increase with depth. This behaviour is similar to that of the macronutrients (TON, phosphate and silicic acid; Fig. 4) and indicates involvement of biological processes in cycling of these elements, with surface water uptake (passive or active) by microbial organisms and deep water remineralisation following vertical transfer of biogenic material to depth (Bruland et al., 2014; Menzel Barraqueta et al., 2018) and/or transport of nutrient-rich deep waters that have collected particles upstream (Middag et al., 2018, 2019); further discussion provided in section on convective supply. The depth distribution of Cd shows strong similarities to those of TON and phosphate, in agreement with other observations (Middag et al., 2018). The distributions of DZn, and to a large extent DAI, showed similarities to silicic acid (Menzel Barraqueta et al., 2018; Middag et al., 2019), potentially suggesting an

involvement in processes related to opal production and dissolution (e.g. by diatoms). The surface removal at station 17 for DCo, DCu and DNi (Fig. 4) was not as pronounced as for DCd and DZn, which is in agreement with other reports and indicated a less pronounced uptake by phytoplankton relative to available stocks in conjunction with a sufficient supply and/or the presence of a fraction of the element which is difficult to assimilate due to ligand binding or slow kinetic dissociation processes (Bruland and Franks, 1983; Martin et al., 1993; Middag et al., 2020). Some combination of these processes is also likely to be responsible for observed residual DCo, DCu and DNi concentrations at depleted nutrient concentrations (non-zero intercepts in element-nutrient plots Figs. S6-8). Iron is presented here to allow comparison to other elements, and shows DFe surface depletion and relatively constant DFe concentrations (0.7-0.9 nM) at depth, with increasing TDFe levels (Achterberg et al., 2018). DMn and DPb also have low surface water concentrations and feature increases in concentrations in the first tens to hundreds of meters of the water column. These trends are likely associated with photoreduction (Mn only; (Sunda et al., 1983)) and remineralisation of sinking material with release of the elements, and the presence of waters perturbed by atmospheric anthropogenic Pb inputs and ventilated over the last decades (mode waters in IRB (0-1000 m), Labrador Seawater (500-2500 m); (Boyle et al., 1986; Zurbrick et al., 2018). A decrease in DMn and DPb concentrations is evident at greater depths and linked to DMn removal through MnO_x formation (Wu et al., 2014), and scavenging of DPb onto particles in addition to presence of water masses less perturbed by historical anthropogenic Pb inputs (Boyle et al., 1986; Echegoyen et al., 2014). High DAl concentrations near the seafloor most likely represents the influence of the nepheloid layer of resuspended sediments, which is also reflected by the very high TDAI and TDFe concentrations (up to 27.2 nM Al and 8.39 nM Fe; Fig. 4) in that part of the water column.

The difference between dissolved and total dissolvable concentrations was relatively small for the so-called 'nutrient-type' elements (Cd, Co, Cu, Ni, Zn) and also Pb, and more pronounced for Al, Mn and Fe (Fig. 4). This is reflected in the contributions of average dissolved to total dissolvable elemental concentration ratios for the full IBIS data set: Al (23%), Mn (66%), Co (74%), Ni (89%), Cd (85%), Pb (88%), Zn (85%), Cu (96%). These findings indicate that in the water column the bio-essential elements (Cd, Cu, Ni, Zn) that are directly involved in microbial functioning, occur largely in the dissolved phase in waters below the euphotic zone as a consequence of rapid remineralisation of sinking biogenic matter with only a minor fraction forming part of biogenic particles. Whereas elements that form an important part of lithogenic (Al), skeletal (Al; (Gehlen et al., 2002)), metal oxide (Mn, Co; (Moffett and Ho, 1996)) material had a larger labile particulate fraction as also reported for Fe (14%; (Achterberg et al., 2013)). The oceanic Pb concentrations are dominated by anthropogenic aerosol inputs (Bridgestock et al., 2016; Wu and Boyle, 1997), with an apparent high solubility of the land-derived combustion related atmospheric aerosols (Chester et al., 1993), and a large fraction of Pb in the dissolved phase in our study region.

A recent GEOTRACES section in the South Pacific (GP16; (Schlitzer et al., 2018)) allows a comprehensive comparison to our study and reports dissolved to total (dissolved+particulate) elemental concentration ratios for open ocean regions remote from land: Zn (ca. 50-98%), Pb (ca. 80-95%), Mn (ca. 66-90%), Cu (90-95%), Co (ca. 80-98%), Cd (ca. 95-99%), Ni (92-99%). Our dissolved:total ratio observations are in good agreement with these South Pacific findings. Particulate elemental

concentrations (Co: up to ca. 2-3 pM, Mn: up to ca. 90 pM, Cd: up to ca. 2-3 pM, Al: up to ca. 4 nM) for a mid-latitude North Atlantic GEOTRACES transect (GA03) (Twining et al., 2015) were also in good agreement with our labile particulate values.

3.4 Ocean sections of dissolved and total dissolvable trace elements

Four transects were sampled at a high spatial resolution in 2010, the first during the spring cruise (D350) and the others during the summer cruise (D354). Sections for dissolved elements for the D354 transects are presented here, and the dissolved elements for D350 and total dissolvable elements for all transects are presented in the SI. The first and second transect were along ca. 60°N, between 20 to 35°W (D350) and 19 to 43°W (D354), respectively, crossing the Reykjanes Ridge at ca. 29°W (Fig. 5, and SI, Fig. S9). The third transect was from 20 to 35°W and 60 to 63°N and crossed the Reykjanes Ridge at about 62°N (Fig. 6). The fourth section was along 60°N from 41.4°W onto the Greenland shelf (Fig. 7).

Figure 5 and Fig. S9 (SI) allow for a comparison between subsurface concentrations (down to ca. 600-800 m) in the IB between spring and summer cruises, during and after the volcanic eruption. In the case of TDFe (Achterberg et al., 2018), higher concentrations were observed in the IB in the top ca. 600 m in spring during the eruption compared to the summer cruise. For the elements which showed a surface water enhancement due to the ash inputs (Al, Mn, Zn; see Fig. 2, and SI Figs. S9-S10), there was no clear evidence of increases in dissolved or total dissolvable concentrations in subsurface waters.

Deep ocean water masses in the study area are all relatively young (i.e. recently ventilated) and have not yet accumulated much remineralised elements and therefore elemental signatures of the water masses are not as pronounced as further south in the Atlantic (e.g. Middag et al., 2018). The nutrient-type elements (Cd, Cu, Ni, Zn) showed increases in dissolved concentrations with depth, also reflected by total dissolvable distributions (see SI Figs. S10, S11, S12). Concentrations of DZn were lowest in Modified North Atlantic Water (MNAW (see SI); 0.3-0.8 nM) and increased gradually (to ca. 1.8-2.0 nM) in deeper Labrador Seawater (LSW), Iceland-Scotland Overflow Water (ISOW) and Denmark Strait Overflow Water (DSOW) (Fig. 5, 6, and SI Text S2 for water masses), in agreement with reports from the GEOTRACES GA02 section (Middag et al., 2019). A shallower increase in DCd was observed, relative to Zn, as also indicated in Fig. 4, with concentrations in the deeper waters reaching ca. 0.24 nM; these observations agree with those (0.2-0.26 nM for North Atlantic Deep Water (NADW) in IRB north of 60°N) reported for the GEOTRACES GA02 section (Middag et al., 2018). Dissolved Cu showed a concentration increase with depth that was intermediate between Zn and Cd, likely related to its hybrid behaviour associated to scavenging upon release following remineralisation (Bruland et al., 2014). Similar DCu trends in the water column are also shown in Cu isotope studies indicating preferential removal of lighter isotopes onto particles (Little et al., 2018; Takano et al., 2014). Nevertheless, the difference between TDCu and DCu was small in deep waters (Fig. 4) indicating a small particulate Cu stock. Deep water DCu concentrations ranged between 1.40-1.60 nM and agree with those reported for the NW Atlantic of 1.70 nmol kg⁻¹ (Bruland and Franks, 1983). Maxima in DCu of ca. 1.70 nM in bottom waters (e.g. Fig. 5), also reflected in TDCu maxima of up to ca. 1.9 nM, were associated with

DSOW and ISOW with likely additional benthic inputs of Cu as suggested by (Boyle et al., 1977), and also indicated in a Cu isotope study (Little et al., 2018). Similar to DCu, the surface water concentrations of DNi were not strongly depleted with concentrations always >1.4 nM. DNi showed a shallower remineralisation compared to DCu, and lower concentrations in the MNAW than the LSW or DSOW/ISOW. The DNi concentration in our study agree well with values ranging between 3.6 and 4.2 nM in DSOW and LSW reported by (Middag et al., 2020). As indicated in Fig. 4, the difference between TDNi and DNi was noticeable and showed that Ni has a larger particulate stock compared with Cd, Cu or Zn. Between ca. 5-20% of TDNi occurred in a reactive particulate form in the water column, with highest fractions in the top of the water column, likely associated with biogenic material. Nevertheless, the remnants of a particulate Ni fraction at depth, indicates that not all Ni is associated with a biogenic fraction that can be readily remineralised by microbial processes. The particulate fraction is unlikely to be lithogenic, as much higher particulate Fe values would be expected throughout the water column than reported for this study (Achterberg et al., 2018). Assuming congruent dissolution of Fe and Ni from crustal origin (Wedepohl, 1991) or ash from the Eyjafjallajökull volcano (Achterberg et al., 2013), this would supply between 1300 and 1600 times more Fe relative to Ni, and there is no evidence of this (see Fig. 5). Particulate Ni therefore appears to be locked up in an unknown organic fraction.

The DAl concentrations ranged between ca. 2 nM in surface waters to 24 nM at depth, with some spatial variability and highest concentrations in the ISOW and DSOW (e.g. Fig. 5), and are in good agreement with those reported (ca. 1.7-23 nM) for the IB and IRB (Menzel Barraqueta et al., 2018). Increases of DAl with depth have been related to sinking opaline material and dissolution at depth as reflected in Si distributions (Gehlen et al., 2002; Menzel Barraqueta et al., 2018), and agree with observations in the Mediterranean (Rolison et al., 2015). Our observations contrast with distributions displaying elevated DAl in surface waters, associated with atmospheric inputs, and decreases with depth related to scavenging, as has been observed in the low latitude North Atlantic (Measures et al., 2015) and Pacific Ocean (Orians and Bruland, 1986).

Enhanced DPb was observed in LSW with concentrations up to ca. 30-40 pM (e.g. Figs. 5 and 7). Similar observations of elevated DPb in LSW have previously been reported (Zurbrick et al., 2018), and attributed to historical atmospheric anthropogenic Pb inputs to the N Atlantic. Lower DPb concentrations in ISOW and DSOW (5-15 pM; Figs. 5 and 6), agree with those reported by (Zurbrick et al., 2018). The dynamic behaviours of Co and Mn, with strong input and removal processes, coupled to the presence of relatively young water masses in the high latitude North Atlantic, meant that no distinct elemental signatures could be observed in the various water masses (Fig. 5, 6).

An important feature along the three deep ocean sections is the elevated concentrations of DMn (up to 0.96 nM), TDMn (up to 3.25 nM), DCo (up to 94 pM), TDCo (up to 135 pM), DAl (up to 19 nM) and TDAI (up to 104 nM) over the Reykjanes Ridge (also associated with enhanced DFe (up to 1.03 nM) and TDFe (up to 57 nM) (Achterberg et al., 2018)), particularly on the eastern flank. The elevated concentrations are likely largely driven by enhanced turbulent mixing over the Reykjanes Ridge with resuspension of sunken particles, with perhaps a contribution by hydrothermal inputs (Achterberg et al., 2018). Internal tides, near-inertial waves and mean flows cause the deep turbulent mixing over the rough topography of mid-

ocean ridges (Clément et al., 2017; St Laurent and Thurnherr, 2007). The mixing over the Reykjanes Ridge will transfer sedimented particulate material into the water column, with associated dynamic exchange of dissolved Mn, Co, Al (and Fe). Removal of DPb through particle scavenging is evident in the vicinity of the Reykjanes Ridge, with concentrations down to 16.5 pM. Similar observations of depleted DPb (ca. 7 pM) have been reported over the mid-Atlantic Ridge (at TAG) for GEOTRACES cruise GA03 (Noble et al., 2015).

The fourth section was from 41.4°W along 60°N onto the Greenland shelf (Fig. 7). The redox sensitive element Mn showed elevated surface dissolved concentrations of 0.35 nM at ca. 60 km off the coast and increasing to >1.35 nM at ca. 30 km off the coast (also see Fig. 3). The DMn increase in coastal waters was coincident with a reduction in salinity indicating the occurrence of EGC waters with reduced temperatures (from 9.14 to 5.83°C) and salinities (from 34.99 to 33.84) as a consequence of freshwater advection south through Fram Strait in addition to local glacier and iceberg melt water inputs from Greenland (Sutherland et al., 2009). The DMn concentrations on the Greenland shelf (200 m water depth) reached >2 nM and were fairly constant below ca. 40 m depth, coinciding with elevated DFe values (up to 1 nM; (Achterberg et al., 2018)) indicating a benthic release of these elements following reductive dissolution (Burdige, 1993). Concentrations of TDMn were also elevated in the Greenland shelf waters and showed an increase near the seafloor to values of 6.83 nM, as a consequence of scavenging/precipitation of DMn diffusing out of the sediments and/or sediment resuspension (SI Fig. S13). The dissolved concentrations of the redox sensitive element Co on the Greenland shelf in the EGC (0.03-0.12 nM) were lower or comparable to subsurface waters off shelf (ca. 0.09-0.11 nM), indicating a low continental and Arctic Ocean supply with limited benthic release and/or important scavenging removal. The TDCo concentrations on the Greenland shelf were between 30% and 300% higher than DCo, indicating an important role for transfer of DCo onto particles (Moffett and Ho, 1996).

Trends in DCd and DZn along this section showed similarities to nutrients, with lower surface levels and an increase with depth. Dissolved Cd showed a pronounced difference between surface and deep water concentrations (e.g. station 13: 0.024 nM surface and 0.22 nM at 300 m). Dissolved Cu and DNi showed elevated concentrations on the Greenland shelf in the EGC, with invariable concentrations with depth and an absence of surface water depletion, likely as a result of enhanced supply and a minimal removal through biological activity.

Dissolved Pb concentrations along the section were similar to other parts of the IB and IRB, and ranged between 0.017-0.03 nM, including concentrations up to 0.024 nM in the EGC, with little depth-related variation, and >80% of Pb in the dissolved phase. The surface water concentrations of DAl ranged between ca. 0.9-2.8 nM with TDAI being up to 10 times higher, and deep water DAl levels increased to 7 nM on shelf and 14 nM off shelf with TDAI being several fold higher.

Clear differences are apparent between the distributions of the various elements. We used principal component analysis (PCA) with the full dataset to determine relationships between various oceanographic variables and hence suggest which processes dominate observed combined trace element distributions in an overall statistical sense (Fig. 8). The first principal component axis (PC1) explains 48% of the

variance and represents mainly depth dependent increases in nutrients and trace elements involved in biological processes and controlled by organic matter production and remineralisation, including DCd, DZn, DCu and DNi but potentially also DPb and DAI. Phosphate and DCd correlate as does Si with both DZn and DAI, in accordance with previous studies (Bruland et al., 2014; Menzel Barraqueta et al., 2018; Middag et al., 2019; Xie et al., 2015). The PCA results also agree with elevated Pearson correlations for the relationships of DCd, DZn, DCu and DNi with depth ($r=0.50, 0.59, 0.45$ and 0.32 , resp.), TON ($r=0.91, 0.51, 0.28$ and 0.39 , resp.), phosphate ($r=0.90, 0.58, 0.42$ and 0.39 , resp.) and silicic acid ($r=0.83, 0.67, 0.43$ and 0.46 , resp.) (SI, Table S3). Enhanced Pearson correlations were observed for the relationships of DPb and DAI with TON ($r=0.46$ and 0.53 , resp.), phosphate ($r=0.46$ and 0.51 , resp.) and silicic acid ($r=0.29$ and 0.75 , resp.) (SI, Table S3). Whilst DPb and DAI distributions are known to be influenced by atmospheric inputs, sediment supply, and scavenging (Measures and Vink, 2000; Menzel Barraqueta et al., 2019; Rusiecka et al., 2018), an association of Al with diatom frustules (Menzel Barraqueta et al., 2018) and Pb with organic matter remineralization and sediment supply (Rusiecka et al., 2018) has recently been reported. A role of Mn and Fe in DPb cycling (but not DAI) is suggested by negative Pearson correlations ($r = -0.45$ and -0.35 for DPb with TDMn and TDFe, resp.) indicating lower DPb at elevated particulate Mn and Fe concentrations related to scavenging.

Dissolved Mn, Co and Fe are micronutrients, and in Fig. 8 fall on the trajectory of the other nutrient-type elements (e.g. Cd), but less of their variance is explained by PC1, indicating that processes other than biological uptake and remineralization influenced their distributions. Whilst these redox sensitive elements have elevated concentrations in oxygen minimum zones as a result of benthic supply (Bruland et al., 2005; Rapp et al., 2019; Schroller-Lomnitz et al., 2019), no association with low oxygen is notable in Fig. 8 and their variance is not explained by the oxygen/salinity correlated PC2. As might be expected, the dissolved concentrations of Mn, Co and Fe therefore appear to be determined by a combination of factors including supply strength, biological uptake and remineralization, characteristics and abundance of particles, and water mass age and mixing.

Plots of nutrients versus trace elements (Figs. S6-S8) confirm the findings of the PCA and Pearson correlations, and show the strong relationships between Si and DZn, and TON/phosphate and DCd. The slopes of the DZn-Si (DZn-PO₄) relationship were 0.084 (0.50) for $<5 \mu\text{M Si}$ ($<0.75 \mu\text{M PO}_4$) and 0.201 (2.79) for $>5 \mu\text{M Si}$ ($>0.75 \mu\text{M PO}_4$), and compare fairly well with slopes of 0.14 (3.0) for waters between 57.5°N and 64°N reported by (Middag et al., 2019) for cruise GA02. Furthermore, the slope of the DNi-PO₄ relationship was 1.04 and compares well with slopes of 1.4 for N Atlantic Central Waters between 50°N and 64°N and 0.6 for North Atlantic Subpolar Mode Waters reported by (Middag et al., 2020). The slope of the DCd-PO₄ relationship was 0.217 and compares well with slopes between 0.2-0.24 for the waters between 50°N and 64°N for GA02 reported by (Middag et al., 2018). The DCd-PO₄ slope is indicative of surface waters and relatively young Atlantic waters with $<1.3 \mu\text{M PO}_4$ and a regression through the origin, with Indian, Pacific and Southern Ocean sourced waters providing a steeper slope and a resulting kink at $>1.3 \mu\text{M PO}_4$ and a regression with a non-zero intercept (de Baar et al., 1994).

3.5 Trace element supply to surface waters of the IB and IRB.

The transfer of trace elements to surface waters for the following sources has been estimated: (i) atmospheric inputs, (ii) winter convective supply, (iii) diffusive fluxes, whilst it is assumed that the horizontal fluxes are small as the horizontal concentration gradients off shelf were relatively minor (also see (Achterberg et al., 2018)).

3.5.1 Atmospheric supply. Atmospheric concentrations of soluble and total trace elements determined using direct aerosol sampling on the spring and summer cruises are presented in Tables 3 and SI Table S4, respectively. The summer cruise observations (fine and coarse fractions combined; Table 3) for soluble Al, Mn, Cu and Ni were within the range of concentrations reported for these elements in remote North Atlantic aerosols from the AMT 18-21 cruises (soluble Al: 25-862 pmol m⁻³, soluble Mn: 0.4-46 pmol m⁻³, soluble Cu, 1.8-22.3 pmol m⁻³, soluble Ni: 1.2-18.4 pmol m⁻³), using the same leaching procedure as our study (Baker and Jickells, 2017). Soluble Zn concentrations were a little lower than those reported by Baker and Jickells (2017) (36-530 pmol m⁻³). Aerosol concentrations in the vicinity of Iceland (between 59.1°N and 62.8°N, 20°W; CLIVAR A16) for deionised water soluble Al ranged between 70-125 pmol m⁻³, Mn between 1.6-2.2 pmol m⁻³ and Pb 0.4-0.6 pmol m⁻³ (Buck et al., 2010), and were therefore similar to our summer cruise observations (fine and coarse fractions combined; Table 3). Reported aerosol concentrations (Shelley et al., 2018) from GEOTRACES cruise GA01 in the high latitude North Atlantic (sample G13, 59.6°N and 38.9°W) for soluble Al (45.9 pmol m⁻³), Ni (0.322 pmol m⁻³), Co (0.005 pmol m⁻³), Cd (0.002 pmol m⁻³) and Pb (0.290 pmol m⁻³) (25% acetic acid leach) were similar to our summer cruise observations (fine and coarse fractions combined; Table 3), but their Mn (0.133 pmol m⁻³), Zn (0.330 pmol m⁻³), Cu (0.107 pmol m⁻³) concentrations were lower than ours. Our observations for soluble trace element concentrations are therefore in reasonable agreement with literature values, whilst recognising that individual observations made during cruises do not reflect the intra-annual variability of aerosol concentrations in the high latitude North Atlantic that can be important (Prospero et al., 2012).

In some cases, soluble element concentrations in the spring non-volcanic samples (TM02-06) were up to several fold (Al, Mn, Pb) or more than an order of magnitude (Cu, Cd) higher than their respective concentrations in the summer. In particular, the concentrations for samples TM04-06 in the IB were above background levels, probably as a result of longer-range transport of ash from the eruption, as indicated by air mass back trajectories (SI Figs. S14-S16). The increases were not consistent with the proportions in which the elements were observed in samples collected under the ash plume, which could possibly be related to changing properties of ejected materials during different phases of eruption, and/or contributions of additional aerosol sources to these spring samples. Size fractionated aerosol soluble Cu, Ni, Co, Cd concentrations for the < 1 µm and > 1 µm fractions observed during the summer cruise were approximately equal at some stations. For soluble Pb, the < 1 µm fraction was ca. 2-6 times higher than the > 1 µm fraction, and for soluble Zn between 1.5-9 times, as also reported by (Arimoto and Duce, 1986; Fomba et al., 2013) and related to their industrial sources from high temperature combustion processes. Concentrations of the soluble Mn fraction of < 1 µm were between 1.1 and 6 times smaller than the > 1 µm fraction, and for soluble Al ranging from equal to 17 times smaller, in accordance with the lithogenic nature of these elements (Arimoto and Duce, 1986; Baker and Jickells, 2017; Fomba et al., 2013).

Rates of dry deposition of soluble trace elements are presented in Table 4, and for many elements (Al, Mn, Co, Cd, Pb) these fluxes were higher by factors of 9 – 113 under the Eyjafjallajokull volcanic ash plume (spring TM07-09) than for all other samples (ratios of median volcanic to median non-volcanic fluxes). The spatial extent of the direct volcanically-derived input fluxes thus appeared to be restricted to waters in the vicinity of Iceland (Achterberg et al., 2013; Gudmundsson et al., 2012). Chemical analysis of Eyjafjallajokull ash collected at sea during cruise D350 indicated 7.91% Al and 0.17% Mn by weight, $173 \mu\text{g g}^{-1}$ Zn, $55.2 \mu\text{g g}^{-1}$ Ni, $4.53 \mu\text{g g}^{-1}$ Pb (sample EYJ 04; SI, Table S5; data from (Achterberg et al., 2013)), consistent with other reports for this material (Gislason et al., 2011) who additionally report on Cu ($35 \mu\text{g g}^{-1}$) and Co ($33 \mu\text{g g}^{-1}$). The solubilities of the aerosol samples (defined as the ratio of soluble to total element concentration) affected by the volcanic emissions were lower compared to other samples (SI, Table S6). However, it should be noted that in some cases (particularly for Ni) total element concentrations were below detection limit and only minimum values for solubility could be determined. For example, the median solubilities of the ash plume samples were 0.92% for Al and 0.96% for Mn, compared to medians of 8.8% and 27% respectively for the other samples. Similar patterns in solubility between the ash and non-volcanic samples were apparent for the other trace elements, with the possible exception of Cd (see SI, Table S6). The soluble trace element inputs to the surface ocean related to ash deposition are likely dominated by a highly soluble salt layer (up to 300 nm) of metal halides and sulphates formed on the ash particles within the volcanic plumes and during their onwards transport through coagulation with aerosol (i.e. SO_4) and the condensation of acidic gases (i.e. SO_2 , HCl, HF) (Duggen et al., 2010; Gislason et al., 2011). The main ash fraction had a mean grain size of $123 \mu\text{m}$ and would have settled through a 30 m mixed layer in ~ 1.5 h (Achterberg et al., 2013), and therefore the short residence time and the relatively low elemental solubilities of the ash limit the inputs for a range of soluble elements including Co, Cd, Cu, Ni and Pb related to the eruption of the Eyjafjallajokull volcano. This is also evidenced by a lack of elevated surface water concentrations for these elements in the vicinity of Iceland during the spring cruise (Fig. 2).

3.5.2 Diffusive vertical fluxes. Diffusive dissolved trace element fluxes were determined during summer 2010 at 21 stations, and the data compiled for annual fluxes in the IB and IRB (Table 5). In general, there was widespread variability in the direction and magnitude of diffusive trace element fluxes, with fluxes both into and out of the mixed layer estimated. The annual diffusive fluxes for the IB and IRB were similar for dissolved Cd and Pb, with three times higher Co fluxes in the IRB and two times lower Mn fluxes in the IRB compared to the IB. The annual fluxes had opposite directions in the IB and IRB for dissolved Ni, Zn, Cu and Al. The variability in annual diffusive fluxes for the various elements was a function of near-surface elemental gradients, which is related to elemental removal by biological uptake and scavenging, and supply by organic matter remineralisation at the base of the mixed layer. Consequently, the overall picture of diffusive elemental supply to surface waters in our study area during summer is variable with no clear geographical or regional patterns.

3.5.3 Convective supply. There is a paucity of data on the winter convective supply of trace elements to surface waters of the high latitude North Atlantic. Annual convective DFe inputs have been reported for the IB (Forryan et al., 2012), and DFe and DAl for our cruise programme covering a wider geographical region, including

both the IB and IRB (Achterberg et al., 2018; Painter et al., 2014), and using a similar technique to Forryan et al. (2012). Here we employed the same approach, and determined convective trace elements inputs to surface waters of the IB and IRB during winter 2010. The convective supply of dissolved Co, Mn, Ni, Cd, Cu, Pb, Zn and Al all showed positive values (Table 5), indicating that subsurface stocks with elevated concentrations were accessed during deep winter mixing, which resulted in a replenishment of depleted surface water stocks. Consequently, the winter mixing was deeper than for example the ferricline or nutricline (Rigby et al., 2020; Tagliabue et al., 2014). This was also the case for the scavenged-type element Mn, which in many ocean regions shows vertical profiles with a depletion with depth due to scavenging, resulting in a dilution by winter mixing of surface water stocks in the Atlantic between 40°S and 40°N (Rigby et al., 2020). The positive Mn supply through convective mixing was related to the surface ocean depletion observed for DMn in this study (Fig. 4) which is then resupplied during winter from deeper water pools. The convective supply rates were remarkably similar for all the elements between the IB and IRB, with typically less than 10% difference, despite differences in deep winter mixing depths (IB 350 m, IRB 200 m). This is in contrast to convective DFe supply, which was nearly four times higher in the IB compared to the IRB (Painter et al., 2014), with the difference related to differences between DFe profiles. Winter mixing depths also change on an interannual basis, with reported depths for the IB of 600 m previously used (Forryan et al., 2012) for DFe convective supply calculations for winter 2007.

the magnitude of estimated convective fluxes indicated that diffusive supply of trace elements was a small supply term to the surface mixed layer relative to convective mixing, ranging from -2.43% for DZn to 13.5% for DCd in the IB to -0.63% for DAl to 6.87% for DCd in the IRB (Table 5). The atmospheric fluxes relative to the combined convective+diffusive fluxes were largest for DAl (9.1% in IB, and 42% in IRB) which has a known atmospheric supply route (Menzel Barraqueta et al., 2019). For the other elements, the atmospheric fluxes were relatively small and less than 4.2% for DZn and 0.13% for DCd, and even less than 2.57% for DPb which has a known atmospheric supply route to the oceans (Boyle et al., 1986, 2014). The observed atmospheric inputs and diffusive vertical fluxes are subject to temporal and spatial variability and have an inherent uncertainty, but overall indicate that these fluxes of dissolved trace elements into the IB and IRB are significantly lower than the fluxes associated with winter mixing.

Convection thus played a dominant role in the supply of dissolved elements to the surface waters, with total supply ratios (relative to P) that were very similar in both basins (Table 2), in agreement with the similarities between supply rates through convection (see above and Table 5). The supply ratios of the various elements are determined by the shape of their vertical profiles and the depth of winter mixing in the respective basin. As a consequence, the trace element: P supply ratios for Zn, Cu, Mn and Fe were similar and ca. 4 times higher than Cd, ca. 10 fold higher than Co, ca. 25-30 times higher than Pb, but ca. 4-7 times lower than Al (Table 2). As mentioned above, the Fe supply ratio was more than 3 times higher in the IB than the IRB, and related to differences in vertical DFe profiles (Achterberg et al., 2018). To first order, total elemental supply ratios were comparable to the apparent removal ratios we calculated between spring and summer (Table 2), suggesting an overall balance between multi-element supply and biologically mediated export stoichiometry in the

region. The reasonable agreement occurred despite the different time windows used for the ratio calculations (spring to summer concentration differences for removal ratio and winter convection for supply ratio). Supply ratios were however generally higher than removal ratios relative to P over the sampled periods (Table 2), with some variability between the trace metals. The overall tendency for supply ratios to exceed removal from spring to summer may reflect preferential remineralisation of the trace metals in these surface waters relative to P (Boyd et al. 2017; Rafter et al. 2017). Further elevated supply ratios relative to removal for the redox sensitive and scavenged-type elements (Fe, Mn, Co, Pb) may then be related to additional dissolved-particle phase processes (colloid formation and scavenging without coinciding P removal, taking place year-round) which will ultimately influence both surface retention (Boyd et al. 2017) and subsurface profiles (Fig. 4) and hence convective re-supply to the surface.

3 Conclusions

This study provides a unique picture of changes from spring to summer in trace element concentrations in the high latitude North Atlantic, a region with pronounced spring blooms and deep water formation. The eruption in spring 2010 of the Eyjafjallajökull volcano resulted in pronounced increases in Al, Mn and Zn in surface waters near Iceland, with concentrations returning to more typical values for the region in summer.

Convective mixing formed the dominant supply mechanism of multiple trace elements to the surface waters, with elemental ratios (relative to P) of convective supply similar to ratios of likely biologically dominated removal. The convective fluxes of bio-essential elements and nutrients would be expected influence magnitude and duration of the high latitude North Atlantic spring bloom, setting an upper bound on export potential from the system (Nielsdottir et al. 2009; Forryan et al 2012; Painter et al. 2014), although additional control by light availability and loss process due to zooplankton grazing could potentially result in this upper bound not being achieved. Interannual variability in the strength of the convective supply might thus influence biological productivity in the region. Over the mid Atlantic ridge, maximum winter mixing depths along 60°N do not usually exceed 300 m (de Boyer Montégut et al., 2004), in agreement with depths down to 400 m as observed at moorings in the central IB (de Jong et al., 2012), however extreme mixing depths of 1 km are possible in cold winters. Therefore, during cold winters the trace element supply to surface waters by convective mixing will be further enhanced. Atmospheric inputs are often considered to form an important source of bio-essential elements to the surface ocean (Duce et al., 1991). However, we show that atmospheric and also diffusive fluxes were low compared to convective fluxes in the high latitude North Atlantic, but nevertheless they provide a sustained trace element supply during the summer period after the winter mixing derived elements may have been depleted.

In contrast, ocean warming is considered to result in upper ocean density stratification. A significant strengthening of stratification (3.3-6.1% increase of mean stratification) has been observed in ~40% of the global ocean since the 1960s (Yamaguchi and Suga, 2019). A shoaling of the maximum depths of winter mixing is projected in climate models as a consequence of the increased stratification (Capotondi et al., 2012). For our study region, assuming it behaves as the global mean, this would likely result in a reduced supply of nutrients and trace elements, and therefore a reduction in productivity and potentially carbon export. Projections for the North Atlantic subpolar

gyre indicated that with a 20% reduction in maximum deep winter mixing depth, a reduced supply of all elements will occur, with the exception of scavenged-type elements, where a reduced dilution of elevated surface ocean stocks might result (Rigby et al., 2020).

Upper ocean stratification is also considered to reduce the transfer of trace elements and nutrients from the deep ocean to the surface mixed layer through upwelling and diapycnal diffusion, as the barrier to transfer across the main thermocline will strengthen (Yamaguchi and Suga, 2019). A reduced advective and diffusive supply of (micro-)nutrients to the surface mixed layer in the subpolar North Atlantic will further enhance the relative importance of seasonal convective mixing, provided that the (micro-) nutrient-clines remain at shallower depths than the maximum winter MLD. Future Icelandic volcanic eruptions could thus have a larger relative impact than presented here for the same deposition magnitude.

Acknowledgements and data

We thank Guantian Li for the TDAI analysis. We thank all the scientists and crew members on IBIS cruises D350/351/354 (RRS *Discovery*, 1962–2012, NERC). We acknowledge M. Stinchcombe for technical support. The authors declare no competing interests. This work was funded by NERC (NE/E006833/1, E.P.A. & C.M.M.), and GEOMAR Helmholtz Centre for Ocean Research Kiel. Data are held at the British Oceanographic Data Centre, <http://www.bodc.ac.uk/>.

References

- Achterberg, E. P., Holland, T. W., Bowie, A. R., Mantoura, R. F. C., and Worsfold, P. J. (2001). Determination of iron in seawater. *Anal. Chim. Acta* 442. doi:10.1016/S0003-2670(01)01091-1.
- Achterberg, E. P., Moore, C. M., Henson, S. A., Steigenberger, S., Stohl, A., Eckhardt, S., et al. (2013). Natural iron fertilization by the Eyjafjallajökull volcanic eruption. *Geophys. Res. Lett.* 40. doi:10.1002/grl.50221.
- Achterberg, E. P., Steigenberger, S., Marsay, C. M., Lemoigne, F. A. C., Painter, S. C., Baker, A. R., et al. (2018). Iron Biogeochemistry in the High Latitude North Atlantic Ocean. *Sci. Rep.* 8. doi:10.1038/s41598-018-19472-1.
- Arimoto, R., and Duce, R. A. (1986). Dry deposition models and the air/sea exchange of trace elements. *J. Geophys. Res.* 91, 2787–2792. doi:10.1029/JD091iD02p02787.
- Bacon, S., Reverdin, G., Rigor, I. G., and Snaith, H. M. (2002). A freshwater jet on the east Greenland shelf. *J. Geophys. Res.* 107. doi:10.1029/2001JC000935.
- Baker, A. R., and Jickells, T. D. (2017). Atmospheric deposition of soluble trace elements along the Atlantic Meridional Transect (AMT). *Prog. Oceanogr.* 158, 41–51. doi:10.1016/j.pocean.2016.10.002.

- Baker, A. R., Weston, K., Kelly, S. D., Voss, M., Streu, P., and Cape, J. N. (2007). Dry and wet deposition of nutrients from the tropical Atlantic atmosphere: Links to primary productivity and nitrogen fixation. *Deep. Res. Part I-Oceanographic Res. Pap.* 54, 1704–1720.
- Birchill, A. J., Hartner, N. T., Kunde, K., Siemering, B., Daniels, C., González-Santana, D., et al. (2019). The eastern extent of seasonal iron limitation in the high latitude North Atlantic Ocean. *Sci. Rep.* 9, 1–12. doi:10.1038/s41598-018-37436-3.
- Bower, A. S., LeCann, B., Rossby, T., Zenk, W., Gould, J., Speer, K., et al. (2002). Directly measured mid-depth circulation in the northeastern North Atlantic Ocean. *Nature* 419, 603–607.
- Boyd, P., Ellwood, M., Tagliabue, A. and Twining, B.S. (2017). Biotic and abiotic retention, recycling and remineralization of metals in the ocean. *Nature Geoscience* 10, 167–173. <https://doi.org/10.1038/ngeo2876>
- Boyd, P. W., Jickells, T., Law, C. S., Blain, S., Boyle, E. A., Buesseler, K. O., et al. (2007). Mesoscale iron enrichment experiments 1993-2005: Synthesis and future directions. *Science*. 315, 612–617.
- Boyle, E. A., Chapnick, S. D., Shen, G. T., and Bacon, M. P. (1986). Temporal variability of lead in the western North Atlantic. *J. Geophys. Res.* 91, 8573. doi:10.1029/JC091iC07p08573.
- Boyle, E. A., Sclater, F. R., and Edmond, J. M. (1977). The distribution of dissolved copper in the Pacific. *Earth Planet. Sci.Lett.* 37, 38–54.
- Boyle, E., Lee, J.-M., Echegoyen, Y., Noble, A., Moos, S., Carrasco, G., et al. (2014). Anthropogenic Lead Emissions in the Ocean: The Evolving Global Experiment. *Oceanography* 27, 69–75. doi:10.5670/oceanog.2014.10.
- Bridgestock, L., van de Flierdt, T., Rehkemper, M., Paul, M., Middag, R., Milne, A., et al. (2016). Return of naturally sourced Pb to Atlantic surface waters. *Nat Commun* 7. doi:10.1038/ncomms12921.
- Brix, H., Gruber, N., Karl, D. M., and Bates, N. R. (2006). On the relationships between primary, net community, and export production in subtropical gyres. *Deep. Res. Part II Top. Stud. Oceanogr.* 53, 698–717. doi:10.1016/j.dsr2.2006.01.024.
- Broecker, W. S. (1991). The Great Ocean Conveyor. *Oceanography* 4, 79–89.
- Brown, M. T., and Bruland, K. W. (2008). An improved flow-injection analysis method for the determination of dissolved aluminum in seawater. *Limnol. Oceanogr.* 6, 87–95.
- Browning, T. J., Al-Hashem, A. A., Hopwood, M. J., Engel, A., Wakefield, E. D., and Achterberg, E. P. (2019). Nutrient regulation of late spring phytoplankton blooms in the midlatitude North Atlantic. *Limnol. Oceanogr.* doi:10.1002/lno.11376.
- Bruland, K., and Franks, R. P. (1983). “Mn, Ni, Cu, Zn and Cd in the Western North Atlantic,” in *Trace Metals in Seawater*, eds. C. S. Wong, E. A. Boyle, K. W.

- Bruland, J. D. Burton, and E. D. Goldberg (New York: Plenum Press), 395–414.
- Bruland, K. W., and Lohan, M. C. (2004). “Controls on trace metals in seawater,” in *Treatise on Geochemistry*, ed. H. Elderfield (London: Elsevier), 23–49.
- Bruland, K. W., Middag, R., and Lohan, M. C. (2014). Controls of Trace Metals in Seawater. *Treatise on Geochemistry*, 19–51. doi:10.1016/B978-0-08-095975-7.00602-1.
- Bruland, K. W., Rue, E. L., Smith, G. J., and Ditullio, G. R. (2005). Iron, macronutrients and diatom blooms in the Peru upwelling regime: brown and blue waters of Peru. *Mar. Chem.* 93, 81–103.
- Buck, C. S., Landing, W. M., Resing, J. A., and Measures, C. I. (2010). The solubility and deposition of aerosol Fe and other trace elements in the North Atlantic Ocean: Observations from the A16N CLIVAR/CO₂ repeat hydrography section. *Mar. Chem.* 120, 57–70. doi:10.1016/j.marchem.2008.08.003.
- Burdige, D. J. (1993). The biogeochemistry of manganese and iron reduction in marine sediments. *Earth-Science Rev.* 35, 249–284.
- Capotondi, A., Alexander, M. A., Bond, N. A., Curchitser, E. N., and Scott, J. D. (2012). Enhanced upper ocean stratification with climate change in the CMIP3 models. *J. Geophys. Res. Ocean.* 117. doi:10.1029/2011JC007409.
- Chester, R., Murphy, K. J. T., Lin, F. J., Berry, A. S., Bradshaw, G. A., and Corcoran, P. A. (1993). Factors Controlling the Solubilities of Trace-Metals from Nonremote Aerosols Deposited to the Sea-Surface by the Dry Deposition Mode. *Mar. Chem.* 42, 107–126.
- Clément, L., Thurnherr, A. M., and St. Laurent, L. C. (2017). Turbulent Mixing in a Deep Fracture Zone on the Mid-Atlantic Ridge. *J. Phys. Oceanogr.* doi:10.1175/JPO-D-16-0264.1.
- de Baar, H. J. W., Saager, P. M., Nolting, R. F., and van der Meer, J. (1994). Cadmium versus phosphate in the world ocean. *Mar. Chem.* 46, 261–281.
- de Boyer Montégut, C., Madec, G., Fischer, A. S., Lazar, A., and Iudicone, D. (2004). Mixed layer depth over the global ocean: An examination of profile data and a profile-based climatology. *J. Geophys. Res.* 109, C12003. doi:10.1029/2004JC002378.
- de Jong, M. F., van Aken, H. M., Vage, K., and Pickart, R. S. (2012). Convective mixing in the central Irminger Sea: 2002 to 2010. *Deep Sea Res. Part I Oceanogr. Res. Pap.* 63, 36–51.
- Duce, R. A., Liss, P. S., Merrill, J. T., Atlas, E. L., Buat-Menard, P., Hicks, B. B., et al. (1991). The atmospheric input of trace species to the world ocean. *Global Biogeochem. Cycles* 5, 193–259. doi:10.1029/91GB01778.
- Duggen, S., Croot, P., Schacht, U., and Hoffmann, L. (2007). Subduction zone volcanic ash can fertilize the surface ocean and stimulate phytoplankton growth: Evidence from biogeochemical experiments and satellite data. *Geophys. Res. Lett.* 34. doi:10.1029/2006gl027522.

- Duggen, S., Olgun, N., Croot, P., Hoffmann, L., Dietze, H., Delmelle, P., et al. (2010). The role of airborne volcanic ash for the surface ocean biogeochemical iron-cycle: a review. *Biogeosciences* 7, 827–844. Available at: <http://www.biogeosciences.net/7/827/2010/>.
- Echegoyen, Y., Boyle, E. A., Lee, J.-M., Gamo, T., Obata, H., and Norisuye, K. (2014). Recent distribution of lead in the Indian Ocean reflects the impact of regional emissions. *Proc. Natl. Acad. Sci. U. S. A.* 111, 15328–31. doi:10.1073/pnas.1417370111.
- Fitzsimmons, J. N., and others (2017). Iron persistence in a distal hydrothermal plume supported by dissolved-particulate exchange. *Nat. Geosci.* 10, 195–201.
- Fomba, K. W., Müller, K., van Pinxteren, D., and Herrmann, H. (2013). Aerosol size-resolved trace metal composition in remote northern tropical Atlantic marine environment: case study Cape Verde islands. *Atmos. Chem. Phys.* 13, 4801–4814. doi:10.5194/acp-13-4801-2013.
- Forryan, A., Martin, A. P., Srokosz, M. A., Popova, E. E., Painter, S. C., and Stinchcombe, M. C. (2012). Turbulent nutrient fluxes in the Iceland Basin. *Deep Sea Res. Part I Oceanogr. Res. Pap.* 63, 20–35. doi:<http://dx.doi.org/10.1016/j.dsr.2011.12.006>.
- Ganzeveld, L., Lelieveld, J., and Roelofs, G.-J. (1998). A dry deposition parameterization for sulfur oxides in a chemistry and general circulation model. *J. Geophys. Res. Atmos.* 103, 5679–5694. doi:10.1029/97JD03077.
- Gehlen, M., Beck, L., Calas, G., Flank, A.-M., Van Bennekom, A. J., and Van Beusekom, J. E. E. (2002). Unraveling the atomic structure of biogenic silica: evidence of the structural association of Al and Si in diatom frustules. *Geochim. Cosmochim. Acta* 66, 1601–1609. doi:10.1016/S0016-7037(01)00877-8.
- Giering, S. L. C., Sanders, R., Achterberg, E. P., Steigenberger, S., Poulto, A., and Mayor, D. J. (2012). Iron recycling by mesozooplankton supports phytoplankton growth in the Irminger Basin. *Geophys. Res. Lett.* 39. doi:10.1029/2012GL051776.
- Gislason, S. R., Hassenkam, T., Nedel, S., Bovet, N., Eiriksdottir, E. S., Alfredsson, H. A., et al. (2011). Characterization of Eyjafjallajökull volcanic ash particles and a protocol for rapid risk assessment. *Proc. Natl. Acad. Sci.* doi:10.1073/pnas.1015053108.
- Grasshoff, K., Ehrhardt, M., and Kremling, K. (1983). *Methods of Seawater Analysis*. Weinheim: Verlag Chemie.
- Graziano, L. M., Geider, R. J., Li, W. K. W., and Olaizola, M. (1996). Nitrogen limitation of North Atlantic phytoplankton: Analysis of physiological condition in nutrient enrichment experiments. *Aquat. Microb. Ecol.* 11, 53–64.
- Gudmundsson, M. T., Thordarson, T., Hoskuldsson, Á., Larsen, G., Björnsson, H., Prata, F. J., et al. (2012). Ash generation and distribution from the April-May 2010 eruption of Eyjafjallajökull, Iceland. *Nat. Sci. Rep.* 2. doi:DOI: 10.1038/srep00572.

- Hamme, R. C., Webley, P. W., Crawford, W. R., Whitney, F. A., DeGrandpre, M. D., Emerson, S. R., et al. (2010). Volcanic ash fuels anomalous plankton bloom in subarctic northeast Pacific. *Geophys. Res. Lett.* 37, L19604. doi:10.1029/2010gl044629.
- Henderson, G. M., Anderson, R. F., Adkins, J., Andersson, P., Boyle, E. A., Cutter, G., et al. (2007). GEOTRACES - An international study of the global marine biogeochemical cycles of trace elements and their isotopes. *Chemie Der Erde-Geochemistry* 67, 85–131.
- Hydes, D. J., Aoyama, M., Aminot, A., Bakker, K., Becker, S., Coverly, S., et al. (2010). Determination of dissolved nutrients (N, P, Si) in seawater with high precision and inter-comparability using gas-segmented continuous flow analysers. , eds. E. M. Hood, C. L. Sabine, and B. M. Sloyan
- Kadko, D. (1993). An assessment of the effect of chemical scavenging within submarine hydrothermal plumes upon ocean geochemistry. *Earth Planet. Sci. Lett.* 120, 361–374. doi:10.1016/0012-821X(93)90250-D.
- Laès, A., Blain, S., Laan, P., Ussher, S. J., Achterberg, E. P., Tréguer, P., et al. (2007). Sources and transport of dissolved iron and manganese along the continental margin of the Bay of Biscay. *Biogeosciences* 4. doi:10.5194/bg-4-181-2007.
- Le Moigne, F. A. C., Moore, C. M., Sanders, R. J., Villa-Alfageme, M., Steigenberger, S., and Achterberg, E. P. (2014). Sequestration efficiency in the iron-limited North Atlantic: Implications for iron supply mode to fertilized blooms. *Geophys. Res. Lett.* 41. doi:10.1002/2014GL060308.
- Lévy, M., Ferrari, R., Franks, P. J. S., Martin, A. P., and Rivière, P. (2012). Bringing physics to life at the submesoscale. *Geophys. Res. Lett.* 39, L14602. doi:10.1029/2012GL052756.
- Lin, I. I., Hu, C., Li, Y.-H., Ho, T.-Y., Fischer, T. P., Wong, G. T. F., et al. (2011). Fertilization potential of volcanic dust in the low-nutrient low-chlorophyll western North Pacific subtropical gyre: Satellite evidence and laboratory study. *Glob. Biogeochem. Cycles* 25, GB1006. doi:10.1029/2009gb003758.
- Little, S. H., Archer, C., Milne, A., Schlosser, C., Achterberg, E. P., Lohan, M. C., et al. (2018). Paired dissolved and particulate phase Cu isotope distributions in the South Atlantic. *Chem. Geol.* doi:10.1016/j.chemgeo.2018.07.022.
- Martin, J. H. (1991). Iron, Liebig's Law, and the Greenhouse. *Oceanography* 4, 53–55.
- Martin, J. H., Fitzwater, S. E., Gordon, R. M., Hunter, C. N., and Tanner, S. J. (1993). Iron, primary production and carbon-nitrogen flux studies during the JGOFS North Atlantic Bloom experiment. *Deep. Res. Part II* 40, 115–134.
- Measures, C., Hatta, M., Fitzsimmons, J., and Morton, P. (2015). Dissolved Al in the zonal N Atlantic section of the US GEOTRACES 2010/2011 cruises and the importance of hydrothermal inputs. *Deep Sea Res. Part II Top. Stud. Oceanogr.* 116, 176–186. doi:10.1016/J.DSR2.2014.07.006.

- Measures, C. I., Landing, W. M., Brown, M. T., and Buck, C. S. (2008). High-resolution Al and Fe data from the Atlantic Ocean CLIVAR-CO2 repeat hydrography A16N transect: Extensive linkages between atmospheric dust and upper ocean geochemistry. *Global Biogeochem. Cycles* 22. doi:Gb100510.1029/2007gb003042.
- Measures, C. I., and Vink, S. (2000). On the use of dissolved aluminium in surface waters to estimate dust deposition to the ocean. *Global Biogeochem. Cycles* 14, 317–327.
- Menzel Barraqueta, J.-L., Klar, J. K., Gledhill, M., Schlosser, C., Shelley, R., Planquette, H. F., et al. (2019). Atmospheric deposition fluxes over the Atlantic Ocean: a GEOTRACES case study. *Biogeosciences* 16, 1525–1542. doi:10.5194/bg-16-1525-2019.
- Menzel Barraqueta, J.-L., Schlosser, C., Planquette, H., Gourain, A., Cheize, M., Boutorh, J., et al. (2018). Aluminium in the North Atlantic Ocean and the Labrador Sea (GEOTRACES GA01 section): roles of continental inputs and biogenic particle removal. *Biogeosciences* 15, 5271–5286. doi:10.5194/bg-15-5271-2018.
- Middag, R., de Baar, H. J. W., and Bruland, K. W. (2019). The Relationships Between Dissolved Zinc and Major Nutrients Phosphate and Silicate Along the GEOTRACES GA02 Transect in the West Atlantic Ocean. *Global Biogeochem. Cycles* 33, 63–84. doi:10.1029/2018GB006034.
- Middag, R., de Baar, H. J. W., Bruland, K. W., and van Heuven, S. M. A. C. (2020). The Distribution of Nickel in the West-Atlantic Ocean, Its Relationship With Phosphate and a Comparison to Cadmium and Zinc. *Front. Mar. Sci.* 7, 105. doi:10.3389/fmars.2020.00105.
- Middag, R., van Heuven, S. M. A. C., Bruland, K. W., and de Baar, H. J. W. (2018). The relationship between cadmium and phosphate in the Atlantic Ocean unravelled. *Earth Planet. Sci. Lett.* 492, 79–88. doi:10.1016/j.epsl.2018.03.046.
- Milne, A., Schlosser, C., Wake, B. D., Achterberg, E. P., Chance, R., Baker, A. R., et al. (2017). Particulate phases are key in controlling dissolved iron concentrations in the (sub)tropical North Atlantic. *Geophys. Res. Lett.* 44. doi:10.1002/2016GL072314.
- Moffett, J. W., and Ho, J. (1996). Oxidation of cobalt and manganese in seawater via a common microbially catalyzed pathway. *Geochim. Cosmochim. Acta* 60, 3415–3424. doi:10.1016/0016-7037(96)00176-7.
- Moore, C. M., Mills, M. M., Milne, A., Langlois, R., Achterberg, E. P., Lochte, K., et al. (2006). Iron limits primary productivity during spring bloom development in the central North Atlantic. *Glob. Chang. Biol.* 12. doi:10.1111/j.1365-2486.2006.01122.x.
- Morel, F. M. M., and Price, N. M. (2003). The biogeochemical cycles of trace metals in the oceans. *Science* (80-). 300, 944–947.
- Nelson, D. M., Brzezinski, M. A., Sigmon, D. E., and Franck, V. M. (2001). A

seasonal progression of Si limitation in the Pacific sector of the Southern Ocean. *Deep Sea Res. Part II Top. Stud. Oceanogr.* 48, 3973–3995. doi:[http://dx.doi.org/10.1016/S0967-0645\(01\)00076-5](http://dx.doi.org/10.1016/S0967-0645(01)00076-5).

- Nielsdottir, M. C., Moore, C. M., Sanders, R., Hinz, D. J., and Achterberg, E. P. (2009). Iron limitation of the postbloom phytoplankton communities in the Iceland Basin, *Global Biogeochem. Cycles* 23. doi:10.1029/2008GB003410.
- Noble, A. E., Echegoyen-Sanz, Y., Ohnemus, D. C., Lam, P. J., Kayser, R., Reuer, M., et al. (2015). Dynamic variability of dissolved Pb and Pb isotope composition from the U.S. North Atlantic GEOTRACES transect. *Deep Sea Res. Part II Top. Stud. Oceanogr.* 116, 208–225. doi:10.1016/J.DSR2.2014.11.011.
- Obata, H., Karatani, H., and Nakayama, E. (1993). Automated determination of iron in seawater by chelating resin concentration and chemiluminescence detection. *Anal. Chem.* 65, 1524–1528.
- Olsen, A., Brown, K. R., Chierici, M., Johannessen, T., and Neill, C. (2008). Sea-surface CO₂ fugacity in the subpolar North Atlantic. *Biogeosciences* 5, 535–547. doi:10.5194/bg-5-535-2008.
- Orians, K. J., and Bruland, K. W. (1986). The biogeochemistry of aluminum in the Pacific Ocean. *Earth Planet. Sci. Lett.* 78, 397–410.
- Painter, S. C., Henson, S. A., Forryan, A., Steigenberger, S., Klar, J., Stinchcombe, M. C., et al. (2014). An assessment of the vertical diffusive flux of iron and other nutrients to the surface waters of the subpolar North Atlantic Ocean. *Biogeosciences* 11. doi:10.5194/bg-11-2113-2014.
- Pickart, R. S., Straneo, F., and Moore, G. W. K. (2003). Is Labrador Sea Water formed in the Irminger basin? *Deep. Res. Part I-Oceanographic Res. Pap.* 50, 23–52.
- Prospero, J. M., Bullard, J. E., and Hodgkins, R. (2012). High-Latitude Dust Over the North Atlantic: Inputs from Icelandic Proglacial Dust Storms. *Science.* 335, 1078–1082. doi:10.1126/science.1217447.
- Rafter, P.A., Sigman, D.M. and Mackey, K.R.M. (2017). Recycled iron fuels new production in the eastern equatorial Pacific Ocean. *Nat Commun* 8, 1100. <https://doi.org/10.1038/s41467-017-01219-7>
- Rapp, I., Schlosser, C., Menzel Barraqueta, J.-L., Wenzel, B., Lüdke, J., Scholten, J., et al. (2019). Controls on redox-sensitive trace metals in the Mauritanian oxygen minimum zone. *Biogeosciences*, 16, 4157-4182. doi.org/10.5194/bg-16-4157-2019.
- Rapp, I., Schlosser, C., Rusiecka, D., Gledhill, M., and Achterberg, E. P. (2017). Automated preconcentration of Fe, Zn, Cu, Ni, Cd, Pb, Co, and Mn in seawater with analysis using high-resolution sector field inductively-coupled plasma mass spectrometry. *Anal. Chim. Acta* 976. doi:10.1016/j.aca.2017.05.008.
- Rigby, S. J., Williams, R. G., Achterberg, E. P., and Tagliabue, A. (2020). Resource Availability and Entrainment are driven by offsets between Nutriclines and

Winter Mixed-Layer Depth. *Global Biogeochem. Cycles* 20.
doi:doi.org/10.1029/2019GB006497.

Rolison, J. M., Middag, R., Stirling, C. H., Rijkenberg, M. J. A., and de Baar, H. J. W. (2015). Zonal distribution of dissolved aluminium in the Mediterranean Sea. *Mar. Chem.* 177, 87–100. doi:10.1016/j.marchem.2015.05.001.

Rosby, T., Prater, M., Zhang, H., Lazarevich, P., and Pérez-Bunius, P. (1998). Isopycnal Float Studies of the Subpolar Front. *WOCE Conf.*

Rusiecka, D., Gledhill, M., Milne, A., Achterberg, E. P., Annett, A. L., Atkinson, S., et al. (2018). Anthropogenic Signatures of Lead in the Northeast Atlantic. *Geophys. Res. Lett.* doi:10.1002/2017GL076825.

Ryan-Keogh, T. J., Macey, A. I., Nielsdottir, M. C., Lucas, M. I., Achterberg, E. P., Bibby, T. S., et al. (2013). Spatial and temporal development of iron stress in relation to phytoplankton bloom dynamics in the high latitude North Atlantic. *Limnol. Oceanogr.* 58, 533–545.

Sanders, R., Brown, L., Henson, S., and Lucas, M. (2005). New production in the Irminger Basin during 2002. *J. Mar. Syst.* 55, 291–310.

Sarmiento, J. L., and Toggweiler, J. R. (1984). A new model for the role of the oceans in determining atmospheric PCO₂. *Nature* 308, 621–624.
doi:10.1038/308621a0.

Schlitzer, R., Anderson, R. F., Dodas, E. M., Lohan, M., Geibert, W., Tagliabue, A., et al. (2018). The GEOTRACES Intermediate Data Product 2017. *Chem. Geol.* doi:10.1016/j.chemgeo.2018.05.040.

Schroller-Lomnitz, U., Hensen, C., Dale, A. W., Scholz, F., Clemens, D., Sommer, S., et al. (2019). Dissolved benthic phosphate, iron and carbon fluxes in the Mauritanian upwelling system and implications for ongoing deoxygenation. *Deep Sea Res. Part I Oceanogr. Res. Pap.* 143, 70–84.
doi:10.1016/J.DSR.2018.11.008.

Shelley, R. U., Landing, W. M., Ussher, S. J., Planquette, H., and Sarthou, G. (2018). Regional trends in the fractional solubility of Fe and other metals from North Atlantic aerosols (GEOTRACES cruises GA01 and GA03) following a two-stage leach. *Biogeosciences* 15, 2271–2288. doi:10.5194/bg-15-2271-2018.

Sholkovitz, E. R., Sedwick, P. N., Church, T. M., Baker, A. R., and Powell, C. F. (2012). Fractional solubility of aerosol iron: Synthesis of a global-scale data set. *Geochim. Cosmochim. Acta* 89, 173–189. doi:10.1016/j.gca.2012.04.022.

St Laurent, L. C., and Thurnherr, A. M. (2007). Intense mixing of lower thermocline water on the crest of the Mid-Atlantic Ridge. *Nature* 448, 680–683.

Sunda, W. G., Huntsman, S. A., and Harvey, G. R. (1983). Photoreduction of manganese oxides in seawater and its geochemical and biological implications. *Nature* 301, 234–236.

Sutherland, D. A., Pickart, R. S., Peter Jones, E., Azetsu-Scott, K., Jane Eert, A., and Ólafsson, J. (2009). Freshwater composition of the waters off southeast

- Greenland and their link to the Arctic Ocean. *J. Geophys. Res.* 114, C05020. doi:10.1029/2008JC004808.
- Tagliabue, A., Mtshali, T., Aumont, O., Bowie, A. R., Klunder, M. B., Roychoudhury, A. N., et al. (2012). A global compilation of dissolved iron measurements: focus on distributions and processes in the Southern Ocean. *Biogeosciences* 9, 2333–2349. doi:10.5194/bg-9-2333-2012.
- Tagliabue, A., Sallee, J.-B., Bowie, A. R., Levy, M., Swart, S., and Boyd, P. W. (2014). Surface-water iron supplies in the Southern Ocean sustained by deep winter mixing. *Nat. Geosci* 7, 314–320. .
- Takano, S., Tanimizu, M., Hirata, T., and Sohrin, Y. (2014). Isotopic constraints on biogeochemical cycling of copper in the ocean. *Nat. Commun.* 5, 1–7. doi:10.1038/ncomms6663.
- Tebo, B. M., Bargar, J. R., Clement, B. G., Dick, G. J., Murray, K. J., Parker, D., et al. (2004). Biogenic manganese oxides: Properties and Mechanisms of Formation. *Annu. Rev. Earth Planet. Sci.* 32, 287–328. doi:10.1146/annurev.earth.32.101802.120213.
- Tomczak, M. (1999). Some historical, theoretical and applied aspects of quantitative water mass analysis. *J. Mar. Res.* 57, 275–303.
- Twining, B. S., and Baines, S. B. (2013). The Trace Metal Composition of Marine Phytoplankton. *Ann. Rev. Mar. Sci.* 5, 191–215. doi:10.1146/annurev-marine-121211-172322.
- Twining, B. S., Rauschenberg, S., Morton, P. L., Ohnemus, D. C., and Lam, P. J. (2015). Comparison of particulate trace element concentrations in the North Atlantic Ocean as determined with discrete bottle sampling and in situ pumping. *Deep Sea Res. Part II Top. Stud. Oceanogr.* 116, 273–282. doi:10.1016/J.DSR2.2014.11.005.
- Vink, S., and Measures, C. I. (2000). The role of dust deposition in determining surface water distributions of Al and Fe in the South West Atlantic. *Deep. Res. I.*
- Wedepohl, K. H. (1991). “The composition of the upper earth’s crust and the natural cycles of selected metals,” in *Metals and their compounds in the environment. Occurrence, analysis and biological relevance*, ed. E. Merian (Weinheim: VCH), 3–65.
- Wu, J., and Boyle, E. A. (1997). Lead in the western North Atlantic Ocean: completed response to leaded gasoline phaseout. *Geochemica Cosmochim. Acta* 61, 3279–3283.
- Wu, J., and Roshan, S. (2015). Cadmium in the North Atlantic: Implication for global cadmium–phosphorus relationship. *Deep Sea Res. Part II Top. Stud. Oceanogr.* 116, 226–239. doi:10.1016/J.DSR2.2014.11.007.
- Wu, J., Roshan, S., and Chen, G. (2014). The distribution of dissolved manganese in the tropical–subtropical North Atlantic during US GEOTRACES 2010 and 2011 cruises. *Mar. Chem.* 166, 9–24. doi:10.1016/J.MARCHEM.2014.08.007.

Wu, J., Sunda, W., Boyle, E. A., and Karl, D. M. (2000). Phosphate Depletion in the Western North Atlantic Ocean. *Science* (80-). 289, 759–762. doi:10.1126/science.289.5480.759.

Wyatt, N. J., Milne, A., Woodward, E. M. S., Rees, A. P., Browning, T. J., Bouman, H. A., et al. (2014). Biogeochemical cycling of dissolved zinc along the GEOTRACES South Atlantic transect GA10 at 40°S. *Global Biogeochem. Cycles* 28, 2013GB004637. doi:10.1002/2013GB004637.

Xie, R. C., Galer, S. J. G., Abouchami, W., Rijkenberg, M. J. A., De Jong, J., de Baar, H. J. W., et al. (2015). The cadmium-phosphate relationship in the western South Atlantic: The importance of mode and intermediate waters on the global systematics. *Mar. Chem.* 177, 110–123.

Yamaguchi, R., and Suga, T. (2019). Trend and Variability in Global Upper-Ocean Stratification Since the 1960s. *J. Geophys. Res. Ocean.* 124, 8933–8948. doi:10.1029/2019JC015439.

Yamazaki, H., and Osborn, T. (1990). Dissipation estimates for stratified turbulence. *J. Geophys. Res.* 95, 9739. doi:10.1029/JC095iC06p09739.

Zurbrick, C. M., Boyle, E. A., Kayser, R. J., Reuer, M. K., Wu, J., Planquette, H., et al. (2018). Dissolved Pb and Pb isotopes in the North Atlantic from the GEOVIDE transect (GEOTRACES GA-01) and their decadal evolution. *Biogeosciences* 15, 4995–5014. doi:10.5194/bg-15-4995-2018.

Accepted

Table 1. Ranges and average concentration values for TON and dissolved and total dissolvable trace elements in surface waters of the high latitude North Atlantic (excluding shelf waters). A regional concentration comparison between the Iceland (IB) and Irminger (IRB) Basins is presented, as well as a seasonal comparison between the spring (D350/351) and summer cruise (D354) of 2010 for each basin; Student t-test was undertaken with a 95% significance threshold. BD: below detection limit.

	Range	Average all (\pm SD)	Average IB (\pm SD)	Average IRB (\pm SD)	t-test (IRB vs IB)	t-test P value (seasonal comparison IB)	t-test P value (seasonal comparison IRB)
Spring cruises							
DCo (pM)	22.9–109	52.8 (\pm 11.0) n = 103	52.2 (\pm 7.49) n = 45	50.7 (\pm 5.65) n = 20	0.40	0.00	0.00
TDCo (pM)	72.2–336	97.4 (\pm 36.1) n = 64	98.4 (\pm 46.5) n = 29	95.6 (\pm 5.29) n = 7	0.75	0.009	0.03
DMn (nM)	0.22–8.73	0.72 (\pm 1.06) n = 103	0.52 (\pm 0.09) n = 45	0.48 (\pm 0.07) n = 20	0.025	0.015	0.006
TDMn (nM)	0.48–10.5	1.42 (\pm 2.14) n = 64	1.12 (\pm 1.83) n = 29	0.77 (\pm 0.39) n = 7	0.098	0.31	0.25
DCd (pM)	36.9–197	125 (\pm 41.7) n = 103	118 (\pm 32.0) n = 45	170 (\pm 17.4) n = 20	0.00	0.00	0.00
TDCd (pM)	102–313	181 (\pm 42.0) n = 69	195 (\pm 47.6) n = 29	170 (\pm 29.7) n = 7	0.098	0.00	0.19
DCu (nM)	0.70–2.28	1.16 (\pm 0.19) n = 103	1.14 (\pm 0.11) n = 45	1.16 (\pm 0.03) n = 20	0.26	0.00	0.00
TDCu (nM)	0.96–2.16	1.21 (\pm 0.23) n = 69	1.17 (\pm 0.15) n = 29	1.21 (\pm 0.06) n = 7	0.30	0.015	0.002
DNi (nM)	1.41–4.14	3.23 (\pm 0.31) n = 103	3.32 (\pm 0.22) n = 45	3.18 (\pm 0.24) n = 20	0.038	0.00	0.00
TDNi (nM)	2.75–7.05	3.80 (\pm 0.48) n = 69	3.76 (\pm 0.16) n = 29	3.91 (\pm 0.09) n = 7	0.0046	0.04	0.85
DZn (nM)	0.07–1.24	0.32 (\pm 0.16) n = 97	0.29 (\pm 0.14) n = 41	0.33 (\pm 0.11) n = 20	0.23	0.00	0.00
TDZn (nM)	0.09–7.19	0.74 (\pm 0.89) n = 64	0.64 (\pm 0.36) n = 28	1.62 (\pm 2.46) n = 7	0.33	0.00	0.23

DAI (nM)	0.27 – 44.8	3.44 (±5.64) n = 105	2.51 (±1.87) n = 45	2.60 (±2.08) n = 20	0.88	0.00	0.00
DPb (pM)	14.8– 36.3	23.4 (±3.87) n = 103	21.9 (±3.33) n = 45	25.0 (±2.02) n = 20	0.00	0.00	0.00
TDPb (pM)	20.9– 99.3	30.7 (±14.2) n = 69	29.3 (±15.6) n = 29	27.7 (±1.97) n = 7	0.59	0.006	0.03
NO₃ (μM)	4.94– 14.5	9.96 (±2.54) n = 94	9.08 (±1.82) n = 43	12.6 (±0.99) n = 19	0.00	0.00	0.00
Summer cruise							
DCo (pM)	20.6– 46.1	37.6 (±11.0) n = 84	32.3 (±5.69) n = 25	40.8 (±11.1) n = 42	0.00		
TDCo (pM)	5.3– 117	75.3 (±23.3) n = 35	71.4 (±9.7) n = 5	76.6 (±30.0) n = 15	0.57		
DMn (nM)	0.24 – 1.35	0.43 (±0.15) n = 84	0.46 (±0.09) n = 25	0.41 (±0.11) n = 20	0.029		
TDMn (nM)	0.03– 1.96	0.72 (±0.31) n = 35	0.76 (±0.16) n = 5	0.69 (±0.28) n = 15	0.49		
DCd (pM)	4.45– 93.7	30.2 (±19.9) n = 87	18.5 (±11.2) n = 26	37.6 (±17.1) n = 44	0.00		
TDCd (pM)	55.9– 274	144 (±62.3) n = 41	107 (±31.6) n = 10	191 (±40.5) n = 15	0.00		
DCu (nM)	0.85 – 1.83	0.97 (±0.14) n = 87	0.93 (±0.04) n = 26	0.99 (±0.13) n = 44	0.006		
TDCu (nM)	0.97 – 1.65	1.10 (±0.11) n = 41	1.08 (±0.07) n = 10	1.09 (±0.04) n = 15	0.62		
DNi (nM)	2.09– 3.44	2.75 (±0.23) n = 85	2.65 (±0.25) n = 26	2.83 (±0.18) n = 42	0.003		
TDNi (nM)	3.11– 4.33	3.72 (±0.32) n = 41	3.53 (±0.29) n = 10	3.89 (±0.25) n = 15	0.004		
DZn (nM)	0.02– 0.23	0.065 (±0.05) n = 68	0.060 (±0.06) n = 19	0.069 (±0.056) n = 37	0.59		

Accepted Article

TDZn (nM)	0.02– 4.65	0.40 (±0.81) n = 34	0.15 (±0.13) n = 5	1.09 (±0.04) n = 15	0.15
DAI (nM)	0.10– 4.81	0.94 (±0.84) n = 89	1.22 (±0.72) n = 26	0.056 (±0.73) n = 43	0.00
DPb (pM)	10.1– 104	17.7 (±9.64) n = 87	16.0 (±2.86) n = 26	16.4 (±1.57) n = 44	0.55
TDPb (pM)	16.8– 37.9	23.7 (±4.3) n = 41	20.6 (±1.9) n = 10	24.6 (±4.3) n = 15	0.004
NO₃ (μM)	BD– 6.47	2.24 (±1.66) n = 74	0.57 (±0.76) n = 21	2.86 (±1.47) n = 40	0.00

Table 2. Removal and supply ratios (in mmol:mol P) of dissolved trace elements relative to P (phosphate) out of and into the surface waters of the Iceland Basin (IB) and Irminger Basin (IRB). Removal ratios were calculated from the differences between spring and summer 2010 surface water concentrations (Table 1), and supply ratios were determined from winter convective mixing (Table 5), which was the dominant supply mechanism for dissolved elements. Dissolved Fe data was obtained from Achterberg et al. (2018) and P supply data (convective mixing) from Painter et al. (2014).

	Removal ratio IB	Removal ratio IRB	Supply ratio IB	Supply ratio IRB
DAI	2.43	4.16	8.24	5.93
DNi	1.26	0.57	4.49	5.03
DZn	0.43	0.43	1.01	1.10
DCu	0.39	0.28	1.24	1.54
DFe	0.27	0.06	0.94	0.25
DCd	0.19	0.22	0.25	0.28
DMn	0.10	0.11	0.81	0.79
DCo	0.037	0.016	0.10	0.11
DPb	0.011	0.014	0.04	0.04

Table 3. Atmospheric trace element soluble concentrations (pmol m^{-3}) during spring and summer 2010. (Spring cruise samples were collected in a single size fraction (Bulk), summer cruise samples were fractionated into particles $<1 \mu\text{m}$ and $>1 \mu\text{m}$. a – Probable contamination). The latitudes and longitudes are the midpoints of aerosol sample collection; dates are at start point of collection. See Fig. S2 (SI) for aerosol sampling map.

	Start Date	Lat.	Long.	Al		Mn		Zn		Cu	
<i>Spring</i>				Bulk		Bulk		Bulk		Bulk	
TM02	28/04/2010	58.39	-20.92	69.6±26.7		1.67±0.48		22.7±4.3		60.6±0.3	
TM03	29/04/2010	59.70	-30.62	190±4.6		10.7±0.29		5.7±1.3		37.0±0.2	
TM04	02/05/2010	59.98	-30.26	479±8.3		9.53±0.62		577±130		218±1.1	
TM05	05/05/2010	60.97	-22.88	425±4.9		11.6±0.54		14.2±4.2		423±2.1	
TM06	07/05/2010	62.50	-19.97	619±10		10.2±0.73		6.8±2.1		26.2±0.2	
TM07	08/05/2010	63.10	-18.75	33586±103		327±9.4		193±31		146±1.2	
TM08	08/05/2010	63.09	-19.08	17760±109		252±7.3		62±19		289±1.7	
TM09	09/05/2010	63.39	-21.31	1280±450		25.6±4.3		<40		147±1.5	
<i>Summer</i>				<1 μm	>1 μm	<1 μm	>1 μm	<1 μm	>1 μm	<1 μm	>1 μm
TM10	17/07/2010	60.00	-38.59	29.7±3.2	28.4±3.6	0.34±0.06	0.38±0.08	9.4±3.4	<2.4	3.6±0.5	0.8±0.4
TM11	19/07/2010	60.72	-38.49	22.6±7.5	67.9±6.5	0.37±0.08	2.06±0.24	14.8±5.4	9.7±2.4	4.8±0.6	6.1±0.4
TM12	23/07/2010	61.19	-32.98	29.9±3.8	512±4	0.45±0.06	1.09±0.12	<9.8	<4.6	1.5±0.5	1.6±0.3
TM13	26/07/2010	59.42	-33.40	95.9±3.7	188.8±4.7	0.35±0.05	1.08±0.08	11.4±2.4	5.0±1.6	1.6±0.3	1.4±0.2
TM14	29/07/2010	63.41	-29.43	1948±96 ^a	204±1.4	6.88±0.34 ^a	0.88±0.06	27.1±2.5 ^a	3.1±0.9	1.6±0.2	0.8±0.4
TM15	04/08/2010	61.18	-22.42	44.8±2.6	82.2±4.0	0.65±0.06	0.82±0.10	<8.7	<5.4	2.0±0.4	1.4±0.7

Table 3 continued.

	Ni		Co		Cd		Pb	
	Bulk		Bulk		Bulk		Bulk	
<i>Spring</i>								
TM02	1.11±0.10		<0.031		13.2±0.34		0.31±0.011	
TM03	<0.25		0.084±0.007		2.35±0.09		1.61±0.01	
TM04	4.53±0.13		0.13±0.02		4.42±0.17		1.14±0.01	
TM05	0.96±0.08		0.12±0.01		4.11±0.13		1.84±0.01	
TM06	0.73±0.14		0.13±0.02		4.48±0.17		1.38±0.01	
TM07	<3.9		1.91±0.30		142±3.6		23.2±0.13	
TM08	2.88±0.78		1.97±0.17		73.3±1.9		10.6±0.08	
TM09	9.3±2.1		<0.60		14.0±2.1		3.41±0.22	
<i>Summer</i>	<1 μm	>1 μm	<1 μm	>1 μm	<1 μm	>1 μm	<1 μm	>1 μm
TM10	0.38±0.15	<0.11	0.086±0.015	0.055±0.013	0.087±0.003	0.011±0.002	0.85±0.06	<0.07
TM11	0.61±0.95	0.88±0.94	<0.050	<0.071	0.15±0.005	0.11±0.003	0.48±0.10	0.32±0.03
TM12	0.83±0.67	0.87±0.36	<0.036	<0.050	0.028±0.004	0.048±0.003	<0.21	<0.07
TM13	0.53±0.53	0.45±0.33	0.11±0.01	0.124±0.01	0.02±0.003	0.015±0.002	<0.15	<0.05
TM14	1.47±0.44	0.72±0.36	0.075±0.01	0.071±0.01	0.12±0.002	0.017±0.001	<0.10	<0.04
TM15	<0.27	0.17±0.27	<0.03	<0.043	0.08±0.003	0.016±0.003	0.24±0.06	<0.06

Table 4. Calculated dry deposition fluxes ($\text{nmol m}^{-2} \text{d}^{-1}$) for soluble metals during the spring and summer cruises. Deposition fluxes are uncertain by a factor of 2-3 (Duce et al., 1991).

	Al	Mn	Zn	Cu	Ni	Co	Cd	Pb
<i>Spring</i>								
TM02	42	1.0	2.0	5.2	0.096	<0.019	1.14	0.027
TM03	115	6.4	0.5	3.2	<0.018	0.051	0.20	0.139
TM04	289	5.8	49.9	18.9	0.391	0.078	0.38	0.098
TM05	257	7.0	1.2	36.5	0.083	0.074	0.35	0.159
TM06	374	6.2	0.6	2.3	<0.084	0.078	0.39	0.119
TM07	20300	198	16.7	12.6	0.218	1.16	12.2	2.00
TM08	10700	152	5.3	25.0	0.249	1.19	6.33	0.911
TM09	774	15.5	<2.9	12.7	0.803	<0.36	1.21	0.295
<i>Summer</i>								
TM10	27	0.4	2.3	1.0	0.105	0.055	0.017	0.115
TM11	61	1.8	9.7	5.6	0.815	<0.065	0.111	0.320
TM12	445	1.0	<4.8	1.5	0.820	<0.047	0.044	<0.080
TM13	171	1.0	5.3	1.4	0.434	0.117	0.015	<0.057
TM14	344	1.4	5.0	0.9	0.744	0.068	0.024	<0.041
TM15	75	0.8	<5.4	1.3	0.167	<0.040	0.021	0.061

Table 5. Annual convective, diffusive and atmospheric trace element fluxes, with their uncertainties. Diffusive and atmospheric fluxes derived from observations made during summer cruise. The convective flux uncertainties are based on the use of mean and standard deviation estimates of the metal concentrations at the winter mixed layer depth of the respective basin. The uncertainties for the atmospheric fluxes are indicated as a range in brackets, with the range being the relevant flux value divided by, and multiplied by, an uncertainty of factor 2 in deposition velocity (Duce et al. 1991). The variability in atmospheric fluxes of the various elements is less than 20% for the samples collected in the respective IB and IRB, and therefore a more realistic flux range is presented based on the deposition velocity uncertainty.

	DCo	DMn	DNi	DCd	DPb	DZn	DCu	DAI
Iceland Basin								
Annual Diffusive Flux ($\mu\text{mol}/\text{m}^2/\text{y}$)		2.07 \pm 0.25	-0.39 \pm 0.94			-0.89 \pm 1.44	-0.78 \pm 0	12.2 \pm 0.13
Annual Diffusive Flux ($\text{nmol}/\text{m}^2/\text{y}$)	55.6 \pm 22.4			1198 \pm 56.1	55.6 \pm 24.6			
Convective Flux ($\text{mmol}/\text{m}^2/\text{y}$)		0.03 \pm 0.01	0.18 \pm 0.02			0.04 \pm 0.02	0.05 \pm 0.01	0.29 \pm 0.05
Convective Flux ($\mu\text{mol}/\text{m}^2/\text{y}$)	3.98 \pm 0.36			8.85 \pm 0.7	1.37 \pm 0.18			
Atmospheric Flux ($\mu\text{mol}/\text{m}^2/\text{y}$)	0.011 (0.006-0.022)	0.28 (0.14-0.56)	0.06 (0.03-0.12)	0.008 (0.004-0.016)	0.012 (0.006-0.024)	1.46 (0.73-2.92)	0.48 (0.24-0.96)	27.3 (13.7-54.6)
Diffusive Flux as % Convective Flux	1.40\pm0.58	6.40\pm2.26	-0.22\pm0.53	13.5\pm1.24	4.05\pm1.86	-2.43\pm4.11	-1.55\pm0.93	4.24\pm0.73
Atmospheric Flux as % Convective+ Diffusive Fluxes	0.27\pm0.34	0.81\pm1.04	0.03\pm0.04	0.08\pm0.12	0.84\pm0.64	4.10\pm3.70	0.98\pm0.94	9.11\pm7.01
Irminger Basin								
Annual Diffusive Flux ($\mu\text{mol}/\text{m}^2/\text{y}$)		1.11 \pm 1.33	0.82 \pm 1.39			2.20 \pm 2.1	0.80 \pm 0.43	-1.04 \pm 2.41
Annual Diffusive Flux ($\text{nmol}/\text{m}^2/\text{y}$)	184 \pm 48.6			706 \pm 321	46.7 \pm 52.2			

Convective Flux (mmol/m ² /y)		0.03±0.001	0.20±0.003			0.04±0.01	0.06±0.003	0.17±0.004
Convective Flux (μmol/m ² /y)	4.18±0.03			10.3±1.03	1.55±0.03			
Atmospheric Flux (μmol/m ² /y)	0.022 (0.011-0.044)	0.38 (0.19-0.76)	0.19 (0.1-0.38)	0.014 (0.007-0.028)	0.041 (0.02-0.084)	1.86 (0.93-3.66)	0.71 (0.35-1.42)	68.4 (34.2-137)
Diffusive Flux as % Convective flux	4.40±1.16	4.08±4.89	0.40±0.67	6.87±3.20	3.02±3.36	5.16±5.09	1.34±0.72	-0.63±1.46
Atmospheric Flux as % Convective+ Diffusive Fluxes	0.50±0.63	1.34±1.67	0.09±0.06	0.13±0.14	2.57±2.01	4.15± 3.27	1.16±1.75	41.7±31.3

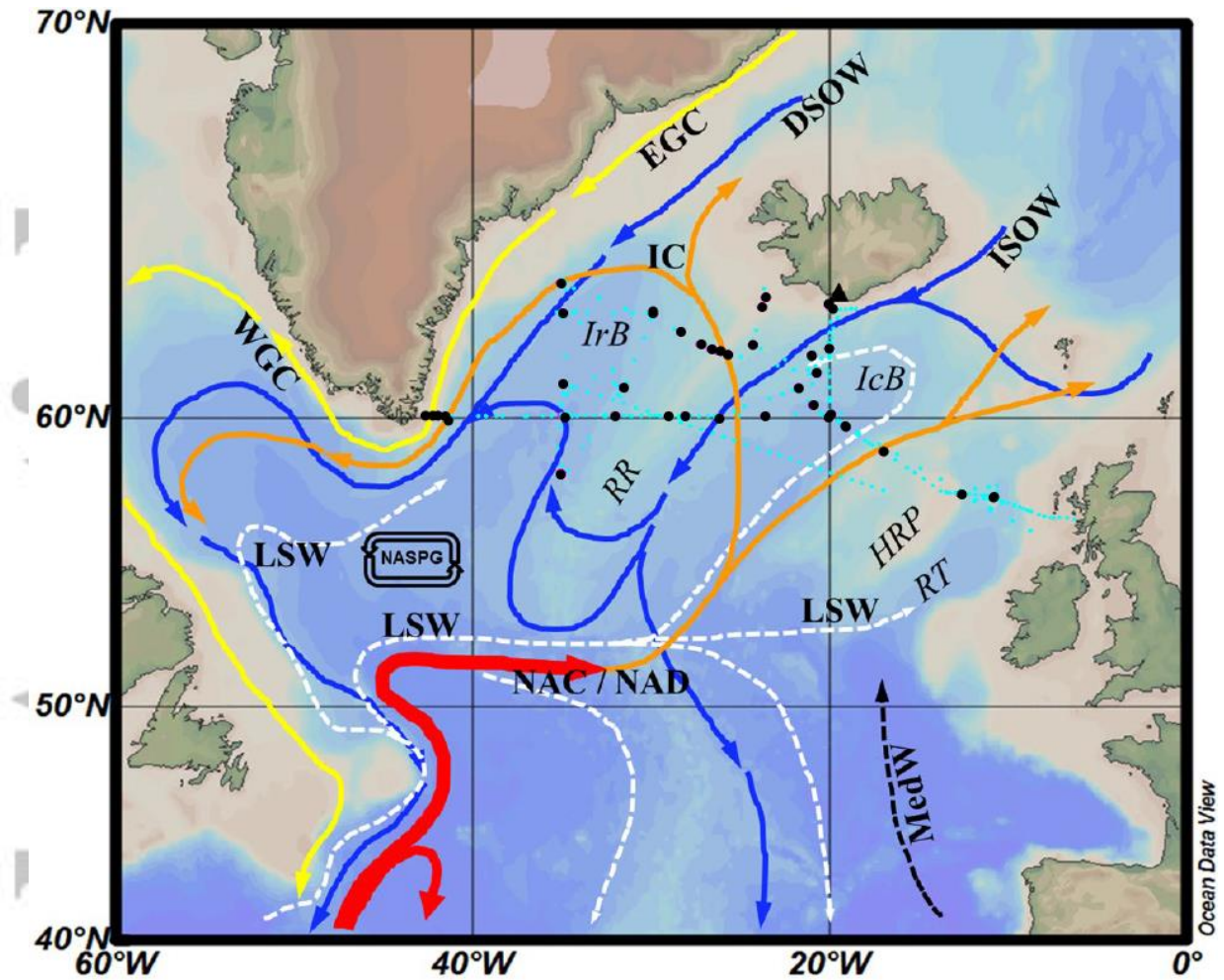


Figure 1. Circulation in the North Atlantic, redrawn from graph originally from IFM-GEOMAR SFB460 overlaid with sampling stations of cruises D350, D351 and D354 (black: CTD, cyan: underway) and the location of the volcano Eyjafjallajökull (black triangle). Red, orange and yellow: near-surface currents. Dashed black and white: intermediate currents. Blue: near-bottom currents. Abbreviations are: LSW: Labrador Sea Water, NAC/NAD: North Atlantic Current/Drift, ISOW: Iceland Scotland Overflow Water, DSOW: Denmark Strait Overflow Water, NASPG: North Atlantic Sub-Polar Gyre, RT: Rockall Trough, HRP: Hatton-Rockall Plateau, IC: Irminger Current, RR: Reykjanes Ridge, IrB: Irminger Basin and IcB: Iceland Basin. Map was produced using Ocean Data View (Schlitzer, R., Ocean Data View, odv.awi.de, 2017).

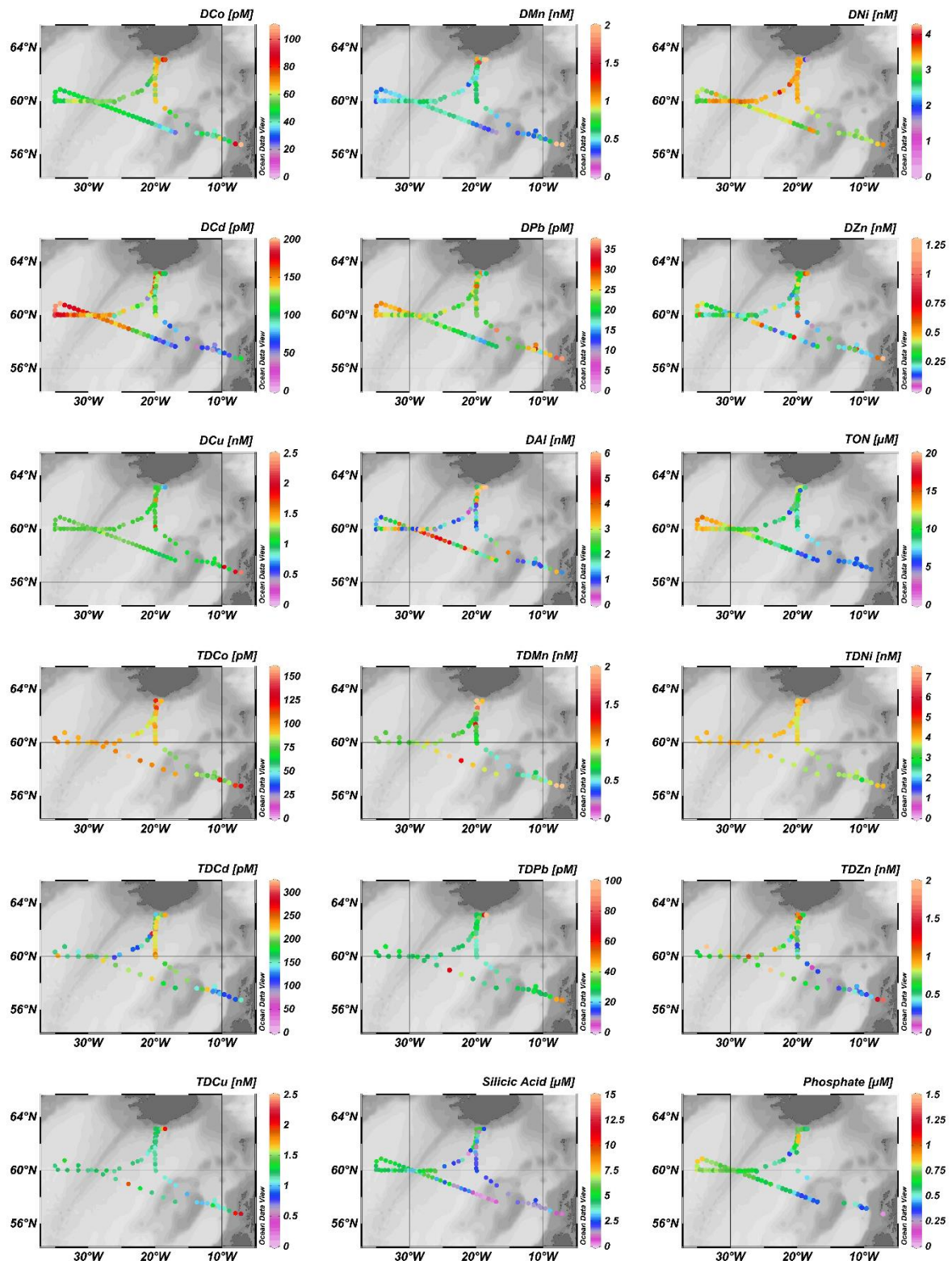


Figure 2: Surface water concentrations (as labelled) of dissolved and total dissolvable Co, Mn, Ni, Cd, Pb, Zn, Cu, Al and nitrate+nitrite (TON), silicic acid and phosphate during spring 2010 (D350&D351). Figures were produced using Ocean Data View (Schlitzer, R., Ocean Data View, odv.awi.de, 2017).

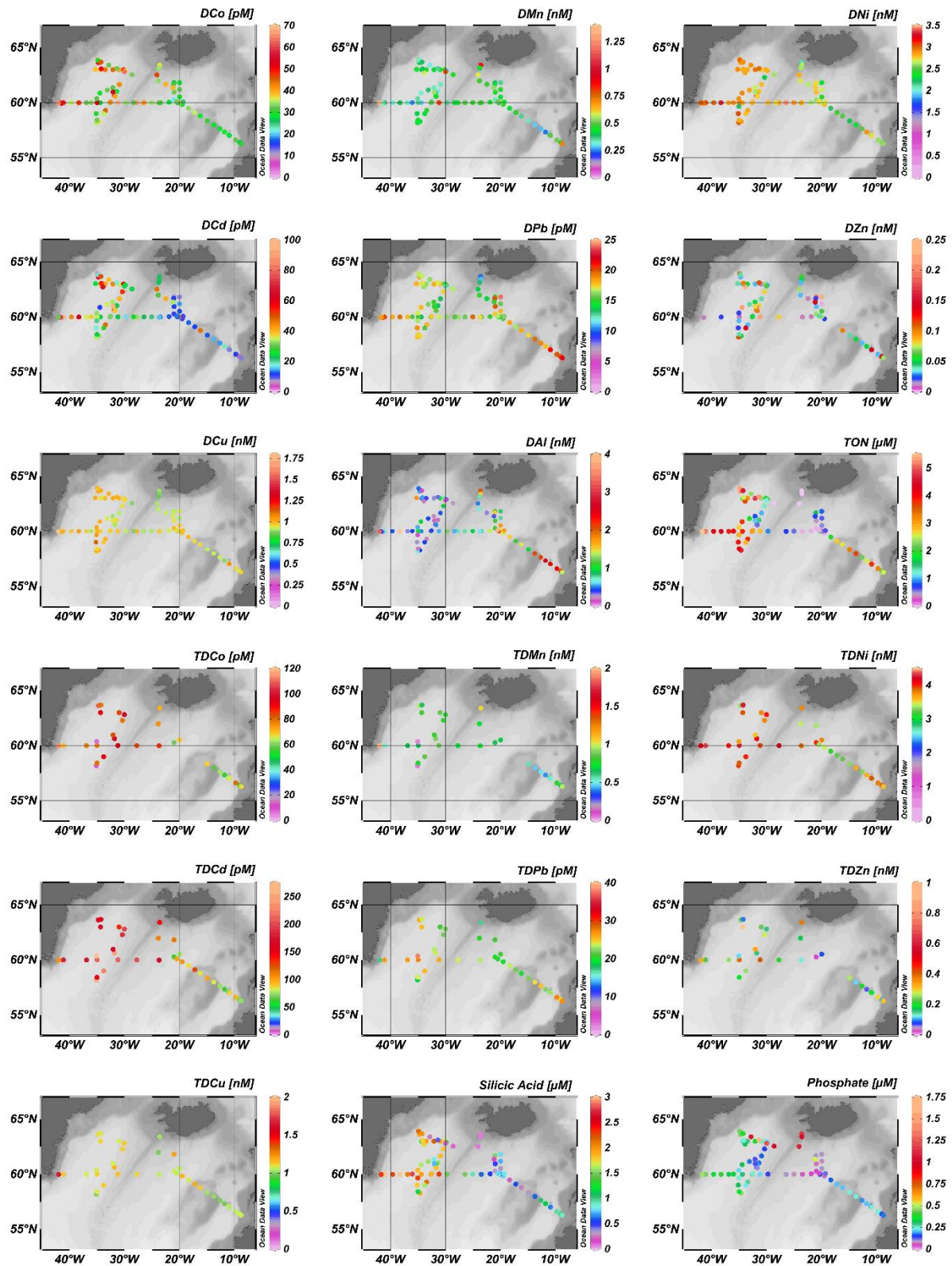


Figure 3: Surface water concentrations (as labelled) of dissolved and total dissolvable Co, Mn, Ni, Cd, Pb, Zn, Cu, Al and nitrate+nitrite (TON), silicic acid and phosphate during summer 2010 (D354). Figures were produced using Ocean Data View (Schlitzer, R., Ocean Data View, odv.awi.de, 2017).

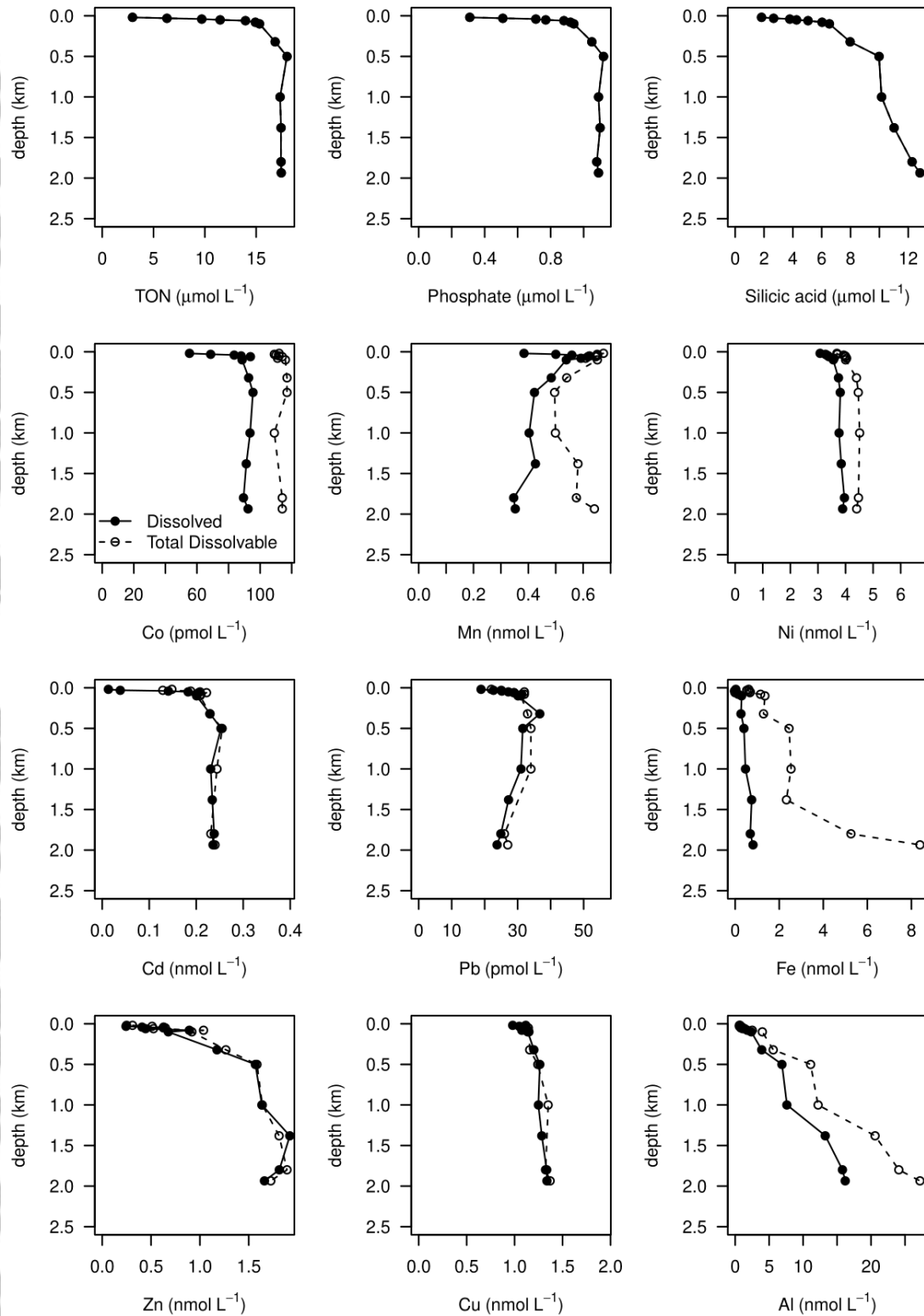


Figure 4: Depth profiles for nitrate+nitrite (TON), phosphate, silicic acid, and dissolved (filled circles) and total dissolvable (open circles) Co, Mn, Ni, Cd, Pb, Fe, Zn, Cu, Al (as labelled) for station 17 (63.01°N, 34.97°W) sampled in IRB during summer 2010 (D354).

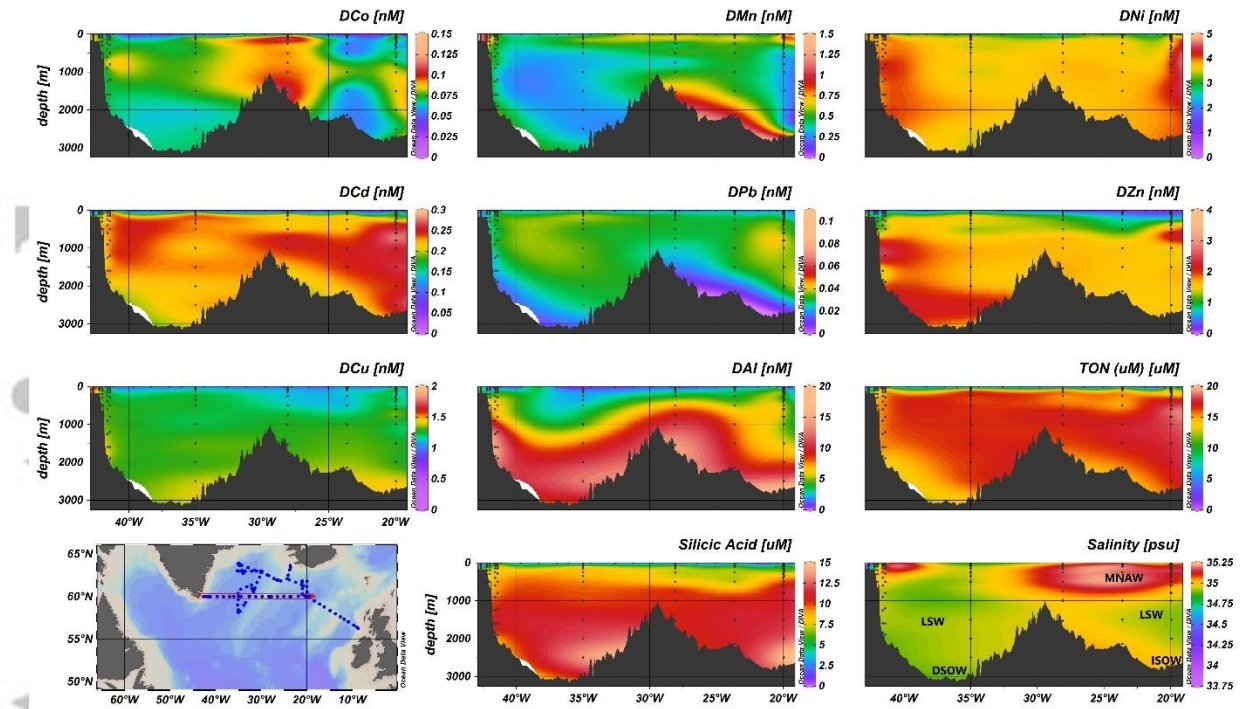


Figure 5: Section plots of dissolved trace elements, nitrate+nitrite (TON), silicic acid and salinity on a transect along 60°N with data from summer 2010. Main water masses indicated in salinity panel and explained in SI Text S2. MNAW: Modified North Atlantic Water; LSW: Labrador Seawater; ISOW: Iceland-Scotland Overflow Water; DSOW: Denmark Strait Overflow Water. Figures were produced using Ocean Data View (Schlitzer, R., Ocean Data View, odv.awi.de, 2017).

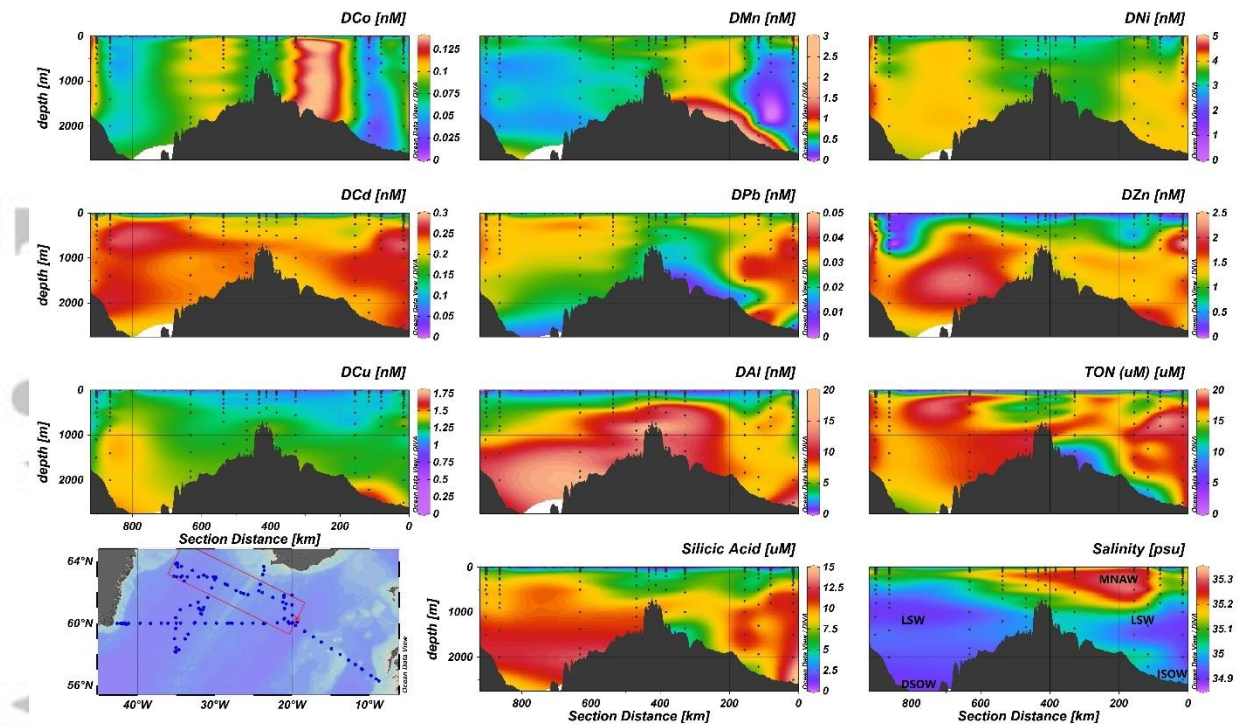


Figure 6: Section plots of dissolved trace elements, nitrate+nitrite (TON), silicic acid and salinity on a transect across the Reykjanes Ridge at 62°N with data from summer 2010. Main water masses indicated in salinity panel and explained in SI Text S2. MNAW: Modified North Atlantic Water; LSW: Labrador Seawater; ISOW: Iceland-Scotland Overflow Water; DSOW: Denmark Strait Overflow Water. Figures were produced using Ocean Data View (Schlitzer, R., Ocean Data View, odv.awi.de, 2017).

Accepted

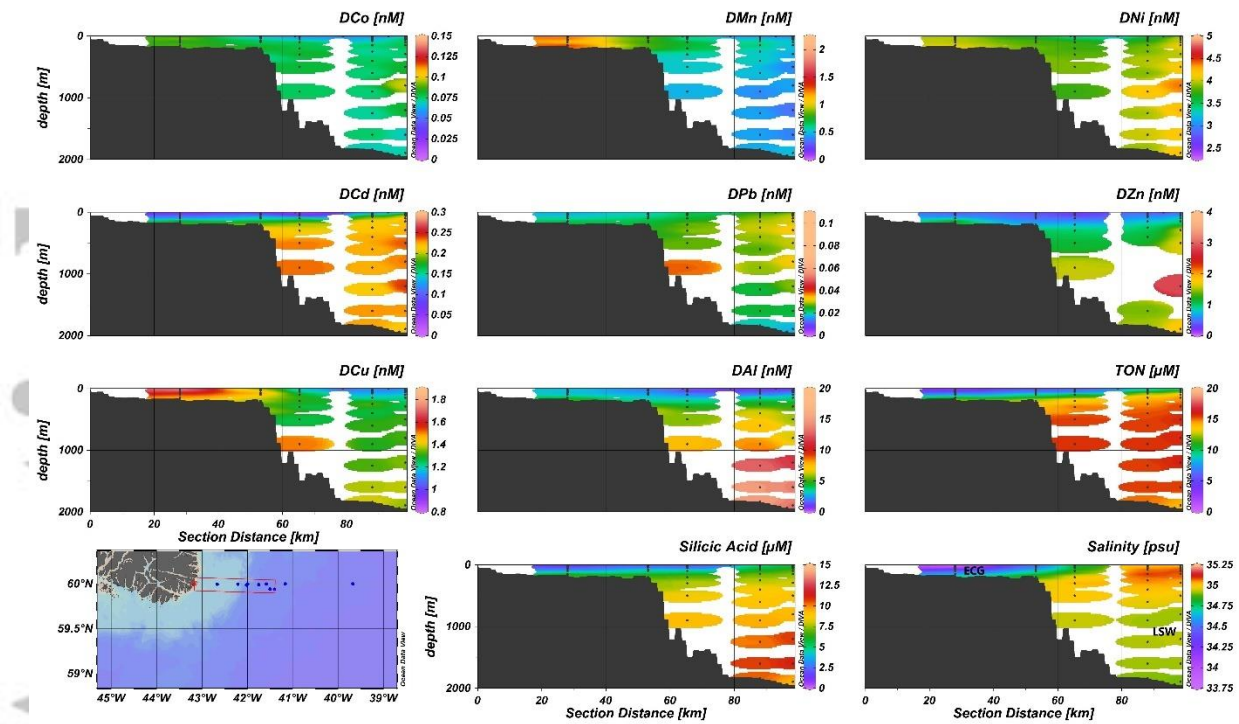


Figure 7: Section plots of dissolved trace elements, nitrate+nitrite (TON), silicic acid and salinity on a transect along 60°N onto the Greenland shelf with data from summer 2010. Main water masses indicated in salinity panel and explained in SI Text S2. ECG: East Greenland Current; LSW: Labrador Seawater. Figures were produced using Ocean Data View (Schlitzer, R., Ocean Data View, odv.awi.de, 2017).

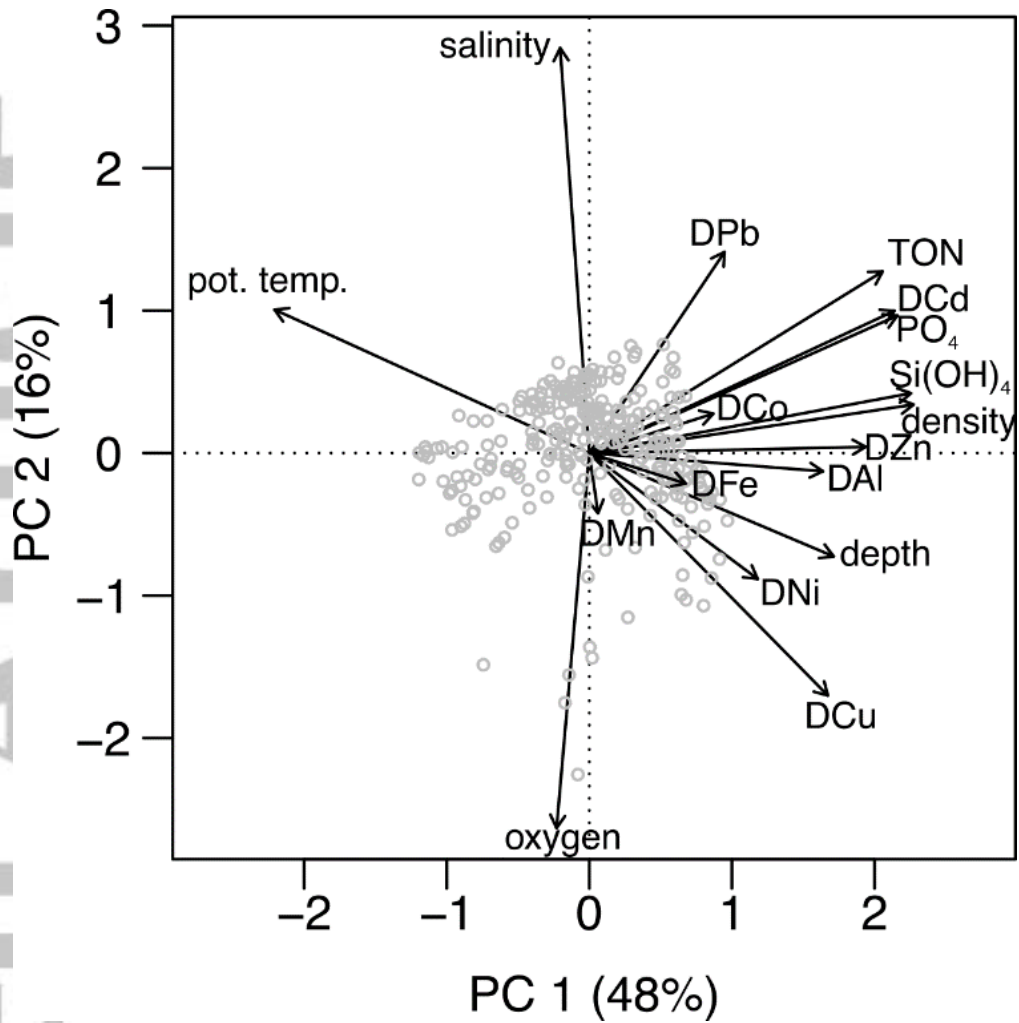


Figure 8: Principal component analysis for IBIS data set. Component scores of each sample are shown as grey circles. Principal component loadings for each variable are shown by black vectors. Loadings/scores have been scaled symmetrically by the square root of eigenvalues.